Sensitivity of aerosol properties to new particle formation mechanism and to primary emissions in a continental scale chemical transport model

Lim-Seok Chang[1], Stephen E. Schwartz, Robert McGraw, Ernie R. Lewis[2]

Atmospheric Sciences Division, Brookhaven National Laboratory, Upton, NY 11973, USA

[1] Present address: National Institute of Environmental Research, Global Environment Research Center, Incheon, 404-708, Korea

[2] To whom correspondence should be addressed: elewis@bnl.gov

Abstract

Four theoretical formulations of new particle formation (NPF) and one empirical formulation are used to examine the sensitivity of observable aerosol properties to NPF formulation and to properties of emitted particles in a continental-scale model for the United States over a one-month simulation (July 2004). For each formulation, the dominant source of Aitken mode particles is NPF with only a minor contribution from primary emissions, whereas for the accumulation mode both emissions and transfer of particles from the Aitken mode are important. The dominant sink of Aitken mode number is coagulation, whereas the dominant sink of accumulation mode number is wet deposition (including cloud processing), with a minor contribution from coagulation. The aerosol mass concentration, which is primarily in the accumulation mode, is relatively insensitive to NPF formulation despite order-of-magnitude differences in the Aitken mode number concentration among the different parameterizations. The dominant sensitivity of accumulation mode number concentration is to the number of emitted particles (for constant mass emission rate). Comparison of modeled aerosol properties with aircraft measurements shows, as expected, better agreement in aerosol mass concentration than in aerosol number concentration for all NPF formulations considered. These comparisons yield instances of rather accurate simulations in the planetary boundary layer, with poor model performance in the free troposphere attributed mainly to lack of representation of biomass burning and/or to long-range transport of particles from outside the model domain. Agreement between model results and measurements is improved by using smaller grid cells (12 km versus 60 km).

1 Introduction

Indirect aerosol forcing, the change in reflected shortwave radiation due to enhancement of cloud drop number concentration and cloud reflectivity by anthropogenic aerosols, remains the largest uncertainty in radiative forcing of climate change over the industrial period (IPCC, 2007). Recent studies have concluded that the main sources of uncertainty in aerosol indirect effects are the uncertainties in cloud parameterization and in aerosol particle number concentration (Menon et al., 2002; Chen and Penner, 2005). As global models often employ empirical or physically based parameterizations to relate cloud droplet number concentration to aerosol number concentration (Boucher and Lohmann, 1995; Kiehl et al., 2000; Ghan et al., 2001, Menon et al., 2002), accurate knowledge of aerosol number concentration and size distribution is important for considerations of the aerosol-cloud interactions in general and of aerosol indirect effects in particular.

The principal processes controlling aerosol number concentration are emission of primary particles, new particle formation (NPF) from vapor precursors, transport, coagulation, and wet and dry deposition. Any uncertainty in representation of these processes in models contributes to uncertainty in modeled aerosol number concentration. Additionally changes in aerosol properties by atmospheric chemical and physical processes affect the dynamics of aerosol particles and in turn their number concentration and size distribution. Aerosol particles can grow or shrink by coagulation, condensation, evaporation, and surface reactions. Coagulation directly reduces concentration of aerosol number (but not mass) and although condensation, evaporation, and surface reactions do not directly alter number concentration, coupling to vapor concentrations and particle growth makes these processes important to considerations of size-dependent number concentration. Accurate knowledge of these processes and representation of their effects in climate models is therefore essential to accurate representation of climate change (Ghan and Schwartz, 2007).

The influence of different processes on overall aerosol number concentration has previously been examined in a term-by-term timescale analysis of the aerosol dynamic equation under typical urban conditions by Zhang and Wexler (2002), who confirmed the intuitive notion that particulate emissions and new particle formation are important determinants of the size distribution of number concentration for urban and regional aerosols. This finding suggests particulate sources as key processes for sensitivity analysis in chemical transport models.

Atmospheric aerosol particles can be classified according to their sources as either primary—those that are injected directly into the atmosphere, and secondary—those that are formed from nucleation of precursor gaseous substances (although both primary and secondary particles can accrete primary and secondary particulate mass by coagulation, condensation, and reaction, somewhat blurring the distinction between primary and secondary particulate matter). Primary aerosol particles commonly provide the dominant contribution to mass concentrations and tend to be considerably larger than secondary aerosol particles, which often dominate number concentrations.

Key examples of primary aerosol particles are sea salt, crustal material (i.e., dust), and anthropogenically emitted particles. Emissions of natural aerosols such as dust and sea salt are strongly dependent on wind speed and surface features, and may occur over large areas, whereas anthropogenic aerosols often arise from point sources. Inventories of anthropogenic emissions, generally developed in support of ambient air quality standards, are based on mass rather than number, and number-based inventories are not anticipated in the near future; consequently, there is little information on the numbers or sizes of primary (i.e., emitted) particles in currently available emissions databases. The impact of emissions on the aerosol size distribution has been investigated by Adams and Seinfeld (2003), who stressed the need for accurate size-resolved emissions.

Secondary aerosol particles evolve from stable nuclei that spontaneously form from vapor precursors and subsequently grow by condensation of vapors and coagulation with other such particles. Here a distinction is made between nucleation and new particle formation: nucleation refers to the formation of stable particles, here taken as diameter 1 nm, whereas new particle formation refers to the production of those nucleated particles that have grown by further condensation of sulfuric acid, ammonia, water, and/or organics or by coagulation with comparably sized particles until they have attained a diameter that is observable by current instrumentation, here taken as 3 nm. The rates of nucleation J and new particle formation J_{NPF} are defined as the number of nucleated particles and new particles, respectively, produced per unit time per unit volume. Because some nuclei are scavenged through coagulation with other nuclei or by larger aerosol particles before attaining the size at which they become new particles, the rate of new particle formation is less than that of nucleation by a factor that depends on the relative importance of the growth rate of the nuclei and the rate at which they are lost to coagulation.

Various mechanisms and formulations for NPF have been proposed. Three mechanisms considered here are binary homogeneous nucleation (BHN) of sulfuric acid and water, ternary homogeneous nucleation (THN) of sulfuric acid, water, and ammonia, and nucleation by ion-ion recombination (NIIR). Formulations for BHN and THN yield rates of nucleation J that depend on the concentration of sulfuric acid molecules $[H_2SO_4]$, the relative humidity RH, the temperature T, and, in the case of THN, the dry air molal mixing ratio of ammonia $[NH_3]$. Nucleation is favored by lower temperatures and higher relative humidities and, in the case of THN, by higher ammonia concentrations, as ammonia neutralizes the sulfuric acid and reduces the energy barrier to nucleation, yielding nucleation rates that can greatly exceed those from BHN under otherwise similar conditions. An alternative mechanism for nucleation is provided by NIIR. According to this mechanism, cosmogenic ions, which are ubiquitous at low concentrations in the atmosphere, can in the presence of typically measured sulfuric acid concentrations lead to the generation of large molecular-ion clusters, which upon recombination with molecular ions of opposite charge yield thermodynamically stable neutral clusters that with further growth can form new particles.

Nucleation parameterizations contain large uncertainties, and debate continues over the mechanisms that dominate, or even operate, under given conditions. As nucleation rates are highly nonlinear in controlling variables (temperature, relative humidity, and concentrations of precursor gases), accurately modeling nucleation occurrence and rates is challenging, as large spatial inhomogeneities of controlling variables within a single to grid cell (typically tens of kilometers on a side) can result in large differences between average nucleation rates over a grid cell and calculated rates based on average values of these variables. Nonetheless the importance of nucleation as a source of new particles warrants investigation of nucleation, new particle formation, and their consequences.

Several model studies have examined nucleation and new particle formation using different assumptions and parameterizations of nucleation rates. Adams and Seinfeld (1992), using a global model, made the assumption that nucleation occurred, if at all, only if the sulfuric acid concentration after condensation onto existing particles was taken into account exceeded a critical value that depended only on temperature and relative humidity. Spracklen et al. (2006), in an investigation of the contribution of boundary layer nucleation events to number concentration on regional and global scales, assumed that nucleation above the boundary layer occurred by BHN, and that in the boundary layer it occurred at a rate that is directly proportional to the concentration of sulfuric acid; the effect of the constant of proportionality was further investigated in a global model by Spracklen et al. (2008). Sotiropoulou et al. (2006) examined air quality and CCN concentrations in a regional model with new particle formation occurring by THN. Parameterizations of new particle formation by binary, ternary, and ion-induced nucleation were examined in a global model by Lucas and Akimoto (2006), who concluded that nucleation parameterizations exhibit large uncertainties arising from inconsistencies between formulations for the same mechanism, numerical fitting errors, and the like. Yu et al. (2008) investigated the importance of ion-mediated nucleation (NIIR) to number concentration in a global model and identified regions where this mechanism would yield large nucleation rates.

The present study examines the effects of uncertainties in parameterizations of nucleation and new particle formation, as well as in numbers and sizes of emitted particles, on the size distribution of aerosol number concentration and on other aerosol properties. Only anthropogenic sources of primary particles (sulfate, nitrate, organic and elemental carbon, and a further, unspecified, category) are considered in this study; dust, sea salt, and biomass burning (which may be anthropogenic) are not included. Because anthropogenic emission inventories are based on mass rather than number, as noted above, models representing aerosol number concentration therefore need to determine number and size distribution of emissions from mass-based inventories until other means become available (Zhang and Wexler, 2004a, b). This situation contributes additional uncertainty to aerosol number concentrations beyond that from the uncertainties in the mass emission inventories themselves. The sensitivity of modeled aerosol number concentrations to this uncertainty in emissions is also examined here.

2 Model Description

The model calculations reported here were carried out using Version 4.4 of the Community Multiscale Air Quality (CMAQ) model (Byun and Ching, 1999; Binkowski, 1999; Binkowski and Roselle, 2003), in which the principal processes affecting aerosol particles that are represented are advection and diffusion, gas-phase chemistry and aqueous sulfate chemistry, aerosol microphysics, aerosol thermodynamics, redistribution of aerosols in convective clouds, and wet and dry deposition.

Gas-phase chemistry is treated using the Statewide Air Pollution Research Center of the University of California at Riverside 1999 (SAPRC99; Carter, 2000) formulation representing volatile organic carbon-nitrogen oxide (VOC-NO_x) chemistry plus oxidation of SO_2 by OH. SAPRC99 as implemented in CMAQ treats 72 species having 214 reactions, involving inorganics (NO_x, O_3, H_2O_2, CO, SO_2, etc.), organics (PANs, 5 lumped alkenes, 2 aromatics, 2 olefins, isoprene, terpenes, etc), and radicals (OH, HO_2, organic peroxy radicals, etc.) of which OH is important as an initiator of sulfuric acid production (as discussed in Section 2.2). Aerosol-forming species are water, sulfuric acid, and ammonia (which are treated here as the sole sources of nucleation), nitric acid, and anthropogenic and biogenic secondary organic aerosol (SOA), which forms from precursors (importantly alkanes, alkenes, aromatics, and monoterpenes) at rates that are derived from experiment (Pandis et al., 1992).

Aqueous sulfate chemistry is based on the Regional Acid Deposition Model (Chang et al., 1987), which treats absorption of gases into cloud droplets, dissociation, oxidation of S(IV) to S(VI), and wet deposition for 11 gaseous species including SO_2, OH, O_3, and H_2O_2, and 12 aerosol species including sulfate, ammonium, and nitrate.

Aerosol microphysics is treated by a modal representation (Binkowski and Roselle, 2003) consisting of three modes (Aitken, accumulation, and coarse) with each mode being characterized by three moments with respect to the dry diameter (i.e., not including water mass). The number concentration in each mode is assumed to have a lognormal distribution, and the three moments are directly proportional to the total concentrations of number, surface area, and volume. Within each mode internal mixing is assumed; that is, all particles within a mode are treated as having the same chemical composition. The moments of the modes are affected by some or all of the following processes: NPF, condensation of sulfuric acid or other gases (besides water vapor), coagulation, and wet and dry deposition. Newly formed particles are treated as entering the Aitken mode, the criterion for which is that subsequent to nucleation the particles have grown to a diameter of 3 nm as discussed above. Condensation can occur in all three modes. Coagulation involving coarse mode particles is assumed to be negligible and is not represented. Aitken mode particles in clouds are assumed to be scavenged by accumulation mode particles (resulting in a decrease in both mass and number concentrations in the Aitken mode, and an increase in mass concentration, but not number concentration, in the accumulation mode) at a constant rate over the cloud lifetime, and unactivated accumulation mode particles can also be scavenged by activated cloud drops (resulting in a reduction of number but not mass concentration in the accumulation mode; this loss is classified as wet deposition rather than coagulation). As new particles grow by condensation of gases and coagulation with other newly formed particles and the mean (dry) diameter of the Aitken mode approaches that of the accumulation mode, in some situations a fraction of each moment of the Aitken mode is transferred to the accumulation mode; this is termed intermodal transfer. This algorithm, discussed below, is formulated here as in Binkowski and Roselle (2003) without modification.

Aerosol thermodynamics is treated by ISORROPIA (Nenes et al., 1998), which calculates the composition and phase state of an ammonium-sulfate-nitrate-chloride-sodium-water inorganic mixture in thermodynamic equilibrium with the corresponding gas-phase precursor species, thus explicitly accounting for the change in size of particles with respect to relative humidity.

The modeling domain covers the continental United States at a resolution of 60 km with 21 vertical levels (based on pressure) extending up to a pressure of 10 hPa (which typically occurs near 30 km); thus the total number of grid cells in the domain is 95×60×21, or approximately $1.2 \cdot 10^5$. Processes in the northeast U.S. are examined in greater detail using a nested domain with a resolution of 12 km. The simulation time was chosen to coincide with the campaign period of the International Consortium for Atmospheric Research on Transport and Transformation

(ICARTT) project, 1 July-31 August, 2004 (Fehsenfeld et al., 2006) to permit comparison with observations.

For the time integration, CMAQ employs operator splitting, in which several processes are performed separately with different time steps, each being dynamically determined based on numerical stability and on the level of accuracy required. The overall time interval, which includes an integral number of time steps for each process, is 15 min; model output was written at every 3 hours. Thus the one-month model run contains ~$3 \cdot 10^3$ time intervals, and output was written 248 times.

2.1 New particle formation

Sensitivity of aerosol number concentration to new particle formation was examined by considering several parameterizations for the rates of nucleation, J, and of new particle formation, J_{NPF}. In addition, one empirical NPF formulation was considered.

Two binary homogeneous nucleation parameterizations were used: that of Jaecker-Voirol and Mirabel (1989), hereinafter BHNJ, and that of Vehkamäki et al. (2002), hereinafter BHNV. The nucleation rate according to BHNJ, J_{BHNJ}, was originally presented graphically and designed for simple interpolation in T and RH. For the present study, graphs of log J_{BHNJ} vs. log [H_2SO_4] for $T = [223, 248, 273, 298, 323]$ K and $RH = [20, 40, 60, 80, 100]$% were scanned, digitized, and fitted to low-order polynomials suitable for multi-linear interpolation. For RH below 10%, a default minimum nucleation rate of 10^{-7} cm^{-3} s^{-1} was used. The expression used for the BHNV nucleation rate, J_{BHNV}, was that presented by Vehkamäki et al. (2002), with stated range of validity $T = 230$-305 K (and extrapolation possible down to 190K), RH from 0.01-100%, and [H_2SO_4] from 10^4-10^{11} cm^{-3}. Vehkamäki et al. stated that for J_{BHNV} from 10^{-6}-10^7 cm^{-3} s^{-1} the parameterization yields rates that are within a factor of 3 of those obtained from the full model.

The parameterization used for the ternary homogeneous nucleation rate, J_{THN}, was that of Napari et al. (2002), who stated that over the range of temperatures 240-300 K, relative humidities 5-95%, [H_2SO_4] from 10^4-10^9 cm^{-3}, [NH_3] from 0.1-100 ppt (parts per trillion, or pmol per mol of dry air), and J_{THN} from 10^{-5}-10^6 cm^{-3} s^{-1}, the parameterized rates are within one order of magnitude of those given by the full theory, with closest agreement at higher values of

J_{THN}. According to Napari et al., classical nucleation theory fails near the binary H_2O-H_2SO_4 limit; therefore, in applying this parameterization here J_{BHNV} was used when $[NH_3] < 0.1$ ppt. Additionally, when $[NH_3] > 100$ ppt or $[H_2SO_4] > 10^9$ cm^{-3}, the value of J_{THN} was set equal to that for $[NH_3] = 100$ ppt and $[H_2SO_4] = 10^9$ cm^{-3}. For values of temperature or RH outside of the range of validity, J_{THN} was set equal to 10^{-5} cm^{-3} s^{-1}, and for $J_{\mathrm{THN}} > 10^6$ cm^{-3} s^{-1} it was arbitrarily set to 10^7 cm^{-3} s^{-1}.

The parameterization used for the rate of nucleation by ion-ion recombination, J_{NIIR}, was that presented by Turco et al. (1998):

$$J_{\mathrm{NIIR}} = Q_{\mathrm{i}} f_{\mathrm{i}} \left(\frac{[\mathrm{H_2SO_4}]}{[\mathrm{H_2SO_4}]_0} \right)^{n*}, \tag{1}$$

where Q_{i} is the local ionization (and recombination) rate, $f_{\mathrm{i}} = 0.001$ is the fraction of recombination events that result in a stable nucleus at a reference vapor concentration $[H_2SO_4]_0 = 5 \cdot 10^6$ cm^{-3}, and $n* = 3$ is the threshold number of sulfuric acid molecules needed to form a stable embryo. It is further required that J_{NIIR} not exceed the ionization rate Q_i. The formulation used for Q_{i} is that of Yu (2002), based on measurements of Millikan et al. (1944) and Neher (1971), which yields an increase from 2 cm^{-3} s^{-1} near Earth's surface to about 30 cm^{-3} s^{-1} at 12 km (near the height of the tropopause), with a more gradual increase with further increase in height.

The nucleation rate J is an upper bound to the rate of new particle formation J_{NPF}, as not all nuclei survive to become new particles, some being scavenged by coagulation on larger particles or on other nuclei before they grow (by condensation and by coagulation with other nuclei) to form detectable new particles, as noted in the introduction. These rates are related by

$$J_{\mathrm{NPF}} = F_{\mathrm{KK}} J, \tag{2}$$

where F_{KK} (≤ 1) is the fraction of initially formed nuclei that grow to become new particles with diameter 3 nm. An analytic formula for F_{KK} was presented by Kerminen and Kulmala (2002) and is used to calculate rates of NPF according to the nucleation parameterizations BHNJ, BHNV, THN, and NIIR. Although the derivation of their expression for F_{KK} is based on several assumptions, especially that self-coagulation of nuclei that are too small to be considered new particles is neglected and that the growth rate of these nuclei (here assumed to occur only through uptake of sulfuric acid, ammonia, or water) is constant, Kerminen and Kulmala stated that this parameterization can be successfully applied provided the nuclei number concentration remains less than 10^5-10^6 cm^{-3}.

An empirically derived expression for J_{NPF} was presented by Eisele and McMurry (1997), hereinafter EM97, based on measurements of rates of NPF at Mauna Lao Observatory, Hawaii and Idaho Hill, Colorado reported by Weber et al. (1996):

$$J_{\mathrm{EM97}} = K[\mathrm{H_2SO_4}]^p \,. \tag{3}$$

A lower bound to the data was given by $p = 1$, and an upper bound by $p = 2$, the latter implying that the nucleation process may be collision-controlled rather than evaporation/condensation-controlled. For the present calculations $p = 2$ and $K = 3.5 \cdot 10^{-15}$ cm^3 s^{-1}, the mean value of those corresponding to the fits shown in EM97 for $p = 2$. As the accuracy of such an empirical expression can be expected to vary considerably, both spatially and temporally, a single set of values (p, K) would not be expected to be appropriate for a region as large as the continental United States; hence the rates obtained from this expression must be treated as representative of potential rates.

The dependence of J_{NPF} on [H_2SO_4] is shown in Fig. 1 for the five NPF parameterizations BHNJ, BHNV, THN, NIIR (each with the factor F_{KK}), and EM97, at 298 K, 50% RH, 10 and 100 ppt of [NH_3], and with no background aerosol and with substantial background aerosol (a lognormal size distribution with $N_{\mathrm{tot}} = 500$ cm^{-3}, geometric standard deviation 1.5, and geometric mean diameter 150 nm). For each NPF parameterization (except for EM97) a minimum background value of J_{NPF} is arbitrarily taken as $1 \cdot 10^{-7}$ cm^{-3} s^{-1}, and a maximum value is arbitrarily taken as $1 \cdot 10^{7}$ cm^{-3} s^{-1}.

The value of [H_2SO_4] that results in a given J_{NPF} depends strongly on the NPF formulation (and on the amount of background aerosol; because H_2SO_4 is scavenged by existing aerosol, NPF is suppressed at high aerosol concentration). Typically this value is the least for EM97 and THN (for [NH_3]=100 ppt), slightly greater for NIIR, several orders of magnitude greater for THN (for [NH_3]=10 ppt), and greater still for BHNJ and BHNV. As the dependence of J_{NPF} on [H_2SO_4] is much stronger for THN (for [NH_3]=100 ppt) than for EM97, when sufficient ammonia is present THN is the dominant nucleation mechanism at values of [H_2SO_4] sufficiently great that appreciable NPF occurs.

2.2 Treatment of sulfuric acid

Sulfuric acid is formed by reaction of OH with SO_2, which, in the presence of water vapor and oxygen, occurs by the overall reaction

$$\mathrm{SO_2 + OH} \rightarrow \ldots \rightarrow \mathrm{H_2SO_4} \tag{R1}$$

with rate k_1[OH][SO_2], where k_1 is a temperature-dependent constant. Sulfuric acid vapor is removed by NPF and by condensation on existing aerosol particles, the latter process occurring at a rate $(-d[\mathrm{H_2SO_4}]/dt)_{\mathrm{cond}} = k_{\mathrm{CS}}[\mathrm{H_2SO_4}]$ with effective first-order rate constant k_{CS}, which depends primarily on the concentrations of surface area in the Aitken and accumulation modes.

In the conventional operator-splitting approach as employed in CMAQ, the sulfuric acid concentration calculated in the chemistry module is introduced into the aerosol nucleation and dynamics modules, where it is partitioned between nucleation and condensation. The approach currently employed in CMAQ assumes that [H_2SO_4] is in steady state with condensation being the only sink:

$$\frac{d[\mathrm{H_2SO_4}]}{dt} = 0 = k_1[\mathrm{OH}][\mathrm{SO_2}] - k_{\mathrm{CS}}[\mathrm{H_2SO_4}], \tag{4}$$

where the first term on the right side represents the average production rate of sulfuric acid molecules over the time interval. When this approach was employed with NPF from both THN and NIIR, it was found that J_{NPF} could be erroneously high and that the amount of sulfuric acid consumed by NPF could become comparable to or exceed the rate of condensation on existing particles, or could even exceed the amount formed. An attempt was made to circumvent this problem by invoking a mass cap—a limit on the amount of H_2SO_4 that can go into new particle formation so that it does not exceed the amount formed.

The probability distribution function of J_{NPF} according to this approach, $dF/d\log J_{\mathrm{NPF}}$, the fraction of occurrences over the entire modeling domain and period that are within a given logarithmic range of J_{NPF}, is shown in Fig. 2a both without and with imposition of the mass cap (the total possible number of occurrences is equal to the number of grid cells in the domain,

~$1.2{\cdot}10^5$, times the number of time intervals in the model run, ~$3{\cdot}10^3$, i.e., ~$4{\cdot}10^8$). The imposition of the mass cap greatly reduces the number of instances of high values of J_{NPF} (Fig. 2a).

To account for the sink of sulfuric acid by NPF, a second approach was employed in which, at steady state, the rate of production of sulfuric acid is set equal to its rate of loss by condensation and new particle formation:

$$\frac{d[\mathrm{H_2SO_4}]}{dt} = 0 = k_1[\mathrm{OH}][\mathrm{SO_2}] - k_{\mathrm{CS}}[\mathrm{H_2SO_4}] - nJ_{\mathrm{NPF}}([\mathrm{H_2SO_4}])\,, \tag{5}$$

where the dependence of J_{NPF} on the sulfuric acid concentration is explicitly shown and n, the number of sulfuric acid molecules in a new particle, is taken as 128 under the assumption that each new particle of diameter 3 nm consists mainly of sulfuric acid. This expression yields a parametric expression for steady state sulfuric acid concentration:

$$[\mathrm{H_2SO_4}] = \frac{k_1[\mathrm{OH}][\mathrm{SO_2}] - nJ_{\mathrm{NPF}}([\mathrm{H_2SO_4}])}{k_{\mathrm{CS}}}\,, \tag{6}$$

which can be solved iteratively for a given formulation of J_{NPF}. Loss of H_2SO_4 was taken into account by initially calculating the rates of consumption of H_2SO_4 by NPF and condensation independently, as if all of the available H_2SO_4 could be consumed by either process alone, and then, if the total H_2SO_4 consumed by the two processes exceeded the total amount available, $[H_2SO_4]$ was decreased, resulting in a decrease in both NPF and condensation rates, until the total available H_2SO_4 was consumed. The problem of over-consumption of $[H_2SO_4]$ was resolved by this approach, as shown by the lack of noticeable change in the probability distribution due to imposition of the mass cap in Fig. 2b.

In some circumstances, however, the steady state assumption is not valid, as when the time constant for approaching steady state is comparable to or greater than the time interval used in the model. Under these circumstances, a third approach was employed in which $[H_2SO_4]$ was evaluated as the average of $[H_2SO_4]$ at the start and the end of a time interval, calculated from

$$\frac{d[\mathrm{H_2SO_4}]}{dt} = k_1[\mathrm{OH}][\mathrm{SO_2}] - k_{\mathrm{CS}}[\mathrm{H_2SO_4}] - nJ_{\mathrm{NPF}}([\mathrm{H_2SO_4}]) \tag{7}$$

rather than by using the steady state assumption. When this third approach was applied the probability distribution (Fig. 2c) exhibited further substantial suppression of NPF relative to that calculated under the steady state assumption (Fig. 2b). This approach to taking into account the time dependence seemed to yield reasonable results and to work over the entire range of J_{NPF} considered, and thus was selected for the present study. Additionally, as J_{NPF} is held constant over each 15 min time interval, the possibility of a more rapid pulse nucleation event is precluded.

In summary, when steady state conditions, in which the rate of production of $[\mathrm{H_2SO_4}]$ is nearly balanced by its loss to condensation and to new particle formation, are rapidly (i.e., within a time step) approached, Eq. 6 is used; otherwise Eq. 7 is solved to find the sulfuric acid concentration. In neither situation is a mass cap employed. It should be noted that NPF is a rare phenomenon, with considerably less than 1% of occurrences exhibiting values of J_{NPF} greater than $1 \cdot 10^{-6}$ cm^{-3} s^{-1}, and even fewer greater than 1 cm^{-3} s^{-1} (Fig. 2c), a value typically taken as that which would produce an appreciable number of new particles. One additional feature visible in each approach is a peak in J_{NPF} near 1 cm^{-3} s^{-1}; this results from NIIR, as is evidenced by the occurrence of this peak when the third approach is applied to nucleation from NIIR alone (Fig. 2d).

2.3 Evolution of particle size

Evolution of particle size in each mode is represented in this model, as in CMAQ, by the rate of change with time of three moments of the size distribution of number concentration with respect to the dry particle diameter: the zeroth moment (which is the same as the number concentration N), the second moment M_2, (directly proportional to the surface area concentration A), and the third moment M_3 (directly proportional to the volume concentration V). Each moment in each mode is transported, preserving the lognormal distribution, as in Binkowski (1999). As the size distribution of number concentration in each mode is assumed to be a lognormal, the geometric mean dry diameter D_{g} and the geometric standard deviation σ_{g} of each mode are related to these moments by

$$D_g = \frac{{M_2}^{3/2}}{N^{5/6}{M_3}^{2/3}} \tag{8}$$

and

$$\ln \sigma_g = \left(\frac{\ln N + 2\ln M_3 - 3\ln M_2}{3} \right)^{1/2} = \left[\ln\left(\frac{N^{1/3}{M_3}^{2/3}}{M_2} \right) \right]^{1/2}, \tag{9}$$

respectively. Major processes affecting the size distribution affect the moments, and hence D_g and σ_g, in different ways. Coagulation of particles within the same mode reduces N and M_2 but leaves M_3 unchanged; because in this process smaller particles attach to larger ones within the same mode, it results in an increase in D_g and a decrease in σ_g. Condensation of gases (other than water vapor) increases M_2 and M_3 but leaves N unchanged, and because smaller particles experience greater relative growth than larger ones, this process also typically results in an increase in D_g and a decrease in σ_g. NPF increases all three moments of the Aitken mode, but especially N, and as the particles that are produced are very small ones, this process results in a decrease in D_g and an increase in σ_g in that mode. Condensation and evaporation of water vapor is taken into account as described above, and particle diameters used in calculations are “wet” diameters, meaning that they are the physical sizes of particles in equilibrium at the ambient relative humidity; however, the diameters and moments are reported as “dry,” meaning that water mass is not included.

Intermodal transfer (IMT) is an artificial process that prevents the Aitken mode from merging into the accumulation mode by transferring some fraction of each of the three moments of the Aitken mode to the accumulation mode at the end of each time interval when certain requirements are fulfilled, namely that both N and the rate of condensational growth of M_3 in the Aitken mode are greater than those in the accumulation mode (Binkowski and Roselle, 2003). This transfer results in a decrease in all three moments in the Aitken mode and an increase of the three moments in the accumulation mode. Because the particles which are transferred are the largest particles in the Aitken mode, and among the smallest in the accumulation mode, IMT results in decreases in D_g of both the Aitken mode and the accumulation mode. The fractions of the moments in the Aitken mode resulting from particles with diameters greater than that for which the corresponding concentrations of both modes are equal are transferred to the accumulation mode with the added imposition that not more than one half of the third moment of the Aitken mode can be transferred at any one time step. As the size distributions of the concentrations in each mode are assumed to be lognormals, the diameters at intersection are readily calculated by solving quadratic equations.

2.4 Input Data to the Regional Model Calculations

Meteorological data used for the chemical transport model calculations (*T*, *RH*, wind speed and direction, cloud and rain properties, and turbulent fluxes) were generated from the Mesoscale Model version 5 (MM5; Dudhia, 1993) with the four-dimensional data assimilation option (which forces the output to conform to observations) on an hourly basis using NCEP (National Centers for Environmental Prediction) reanalysis for the continental U.S. with horizontal resolution of 60 km for the continental scale domain and 12 km for the northeastern U.S. These data were then input into the Meteorology-Chemistry Interface Processor (MCIP; Byun et al., 1999), which links MM5 to CMAQ in terms of data format, units, and reconstruction on a different grid structure. MCIP also enforces consistency among the meteorological variables such as height of the planetary boundary layer and cloud parameters.

Anthropogenic emissions (gas and particulate) were based on the Environmental Protection Agency (EPA) 1999 National Emission Inventory (NEI99) updated for a typical summer day of 2004 using projected and known changes for the previous 5 years according to McKeen et al. (2005). In particular, Canadian area sources are included south of 52°N but Canadian point sources are not included in this inventory. This revised inventory was previously used for evaluation of air quality forecast models in the ICARTT field study (Fehsenfeld et al., 2006). The primary emitted species are NO, NO_2, VOC, CO, SO_2, NH_3, PM2.5, and PM10, along with 41 speciated VOC compounds and 5 PM2.5 aerosol species (sulfate, nitrate, organic carbon, elemental carbon, and unspecified PM2.5). Dimethylsulfide (DMS), a marine indirect source of SO_2 through its oxidation, was not treated in this study, thus precluding any potential contribution to $[H_2SO_4]$ (through oxidation of SO_2) and hence nucleation from this source. The inventory was transformed by the Sparse Matrix Operator Kernel Emissions (SMOKE) modeling system (available at http://www.baronams.com/products/smoke/) to hourly gridded emission rates at a resolution of 4 km, which were remapped to the grid sizes employed in the two model domains (60 km and 12 km). Area sources were assigned to the lowest vertical level and point sources to specific vertical layers depending on quantities such as stack height, plume rise, and vertical dispersion. Emissions that are introduced in a single grid cell in the model are treated as uniformly distributed over the cell.

The emission inventory for primary particles contains no information on their sizes. In the current study the size distributions of emitted mass are treated as lognormals with dry geometric mean diameters of 30 nm, 300 nm, and 6 μm and geometric standard deviations of 1.7, 2.0, and 2.2 for the Aitken, accumulation, and coarse modes, respectively. The corresponding size distributions of aerosol number emissions in these three modes are therefore also lognormals with dry geometric mean diameters near 13, 71, and 930 nm, respectively, and the same geometric standard deviations as for the mass emissions. The consequences of these assumptions, especially for geometric mean diameters, are examined below. The partitioning of each species between modes follows the CMAQ approach of putting 99.9% of total emitted mass into the accumulation mode and 0.1% into the Aitken mode, both in the dry state (this is equivalent to assuming that nearly twice as many particles are emitted into the accumulation mode as into the Aitken mode); the consequences of this choice are also discussed below. The coarse mode emissions are based on the difference of PM10 and PM2.5. No explicit emission of dust or sea salt particles, which would be mainly in the coarse mode, is treated in the present model; thus the condensation sink in the model might be less than what it would be in situations and locations for which these particles would otherwise contribute.

Rates of biogenic emissions of gases were obtained from the Biogenic Emissions Inventory System (BEIS) version 3.11, developed by the U.S. Environmental Protection Agency (described at http://www.epa.gov/asmdnerl/biogen.html). Emissions of isoprene, monoterpenes, other organic VOC, and NO were partitioned into the appropriate SAPRC-99 species according to meteorological conditions. Emissions from biomass burning were not included in source inventories.

The spatial distributions of emission fluxes of sulfur dioxide and ammonia, which are precursors for NPF, are shown in Fig. 3 for 1 July 2004. Emission fluxes of sulfur dioxide were high over the eastern U.S., mainly because of the density of power plants there. In contrast, emission fluxes of ammonia were high over the mid-continental U.S., where agriculture activities and livestock husbandry are centered.

3 Experiments

The sensitivities of aerosol number concentration to NPF and primary emission were examined using nine model variants as listed in Table 1. Sensitivity to NPF formulation was examined by comparing the base case (denoted BASE), for which the sole source of particles was primary emission (i.e., no NPF), to two BHN formulations (BHNJ and BHNV), one THN formulation, and NIIR (for all of which the conversion factor F_{KK} was employed to yield J_{NPF}), and one empirically derived parameterization for J_{NPF} (EM97), each of which was examined in a separate model run. Sensitivity to the number (size) of emitted particles was examined by comparing results for the NPF mechanism being the sum of THN and NIIR with the emissions as described above (D_0 case) to those for which the dry diameters of the emitted particles were decreased and increased by a factor of two ($D/2$ and $D\times2$ cases, respectively) while holding the mass emissions constant. In each case the model was run for two months, the first with no nucleation and the second with nucleation, before the time period of interest. The model was initialized using a typical profile of chemical species provided by CMAQ (thus no intercontinental transport of pollutants nor any downward transport of ozone from the stratosphere was included).

3.1 Sensitivity to NPF formulation

The dependence of aerosol number concentration and properties on NPF formulation was investigated by analyzing in detail model results at four sites, chosen to represent typical values for different parameters that might affect NPF. These sites are shown in Fig. 4 along with the simulated wind field, averaged over July, 2004, at an elevation corresponding to 85% of the surface pressure (near 1.5 km). Site A, near the northwestern corner of Iowa, is a rural location surrounded by intensely fertilized agriculture and is characterized by high [NH_3]. Site B, near New Haven, Connecticut, is an urban site that is strongly impacted by upwind urban emissions. Site C, near Acadia National Park, Maine, is a location that is frequently subject to transport of material from urban locations, although further removed than Site B. Site D, 350 km southeast of Cape Cod, Massachusetts, is a marine location well removed from local continental sources. Time series of J_{NPF} and controlling variables (T, RH, [SO_2], [NH_3], and [H_2SO_4]), number concentrations in the Aitken (N_{ATK}) and accumulation (N_{ACC}) modes, and other related quantities for each NPF formulation at the lowest model level (0-20 m above the ground) at each of the four locations are shown in Fig. 5a-d. As noted above, values of $D_{\mathrm{g,ATK}}$, $D_{\mathrm{g,ACC}}$, and the volume concentration in the Aitken mode V_{ATK} are reported for the dry particles (i.e., without taking into account the associated water), although in the calculation of processes such as dry deposition and coagulation the actual (i.e., wet) sizes, which included the associated water, were used.

The behavior of factors affecting NPF differed appreciably between the sites. Temperatures at sites A and B exhibited considerable variability and had pronounced diurnal cycles, as opposed to those at sites C (which were consistently lower than the others) and D. Relative humidities at sites A and B likewise exhibited considerable variability and had pronounced diurnal cycles, whereas those at sites C and D were consistently higher and much more uniform, reflecting the coastal or marine locations of these sites. The concentrations of SO_2 at site B were considerably higher than those at the other sites (note the different axis scale for [SO_2] for that site), whereas those at sites C and D were often negligible, with only occasional instances of nonnegligible values. The concentrations of NH_3 at site A were considerably higher than those at the other sites (note also the different axis scales for [NH_3] for each site), which were frequently negligible. Thus it was expected that NPF at these sites by the several formulations examined here would exhibit substantial differences, both in frequency and amount, allowing differences in controlling processes to be identified and their sensitivities examined.

Several features were common among all sites. The concentration of sulfuric acid exhibited a strong diurnal profile, generally peaking around local noon, reflecting the photochemical production of OH and the short lifetime of this species. As NPF requires the presence of H_2SO_4, both F_{KK} and J_{NPF} for each of the formulations (when NPF occurred) also exhibited a diurnal profile, but with the magnitude of J_{NPF}, or whether NPF occurred at all, depending on location and, at a given location, on the NPF formulation. For instance, because THN is governed by the availability of NH_3, NPF by THN occurred mainly in regions with appreciable [NH_3]. As NPF results in new particles in the Aitken mode, N_{ATK} likewise exhibited a strong diurnal pattern when NPF occurred, but with a somewhat asymmetric or saw-tooth profile reflecting the abrupt onset of NPF followed by a slower decay of N_{ATK} due to coagulation and/or intermodal transfer. Self-coagulation of Aitken mode particles also exhibited a diurnal profile, but with the maxima occurring slightly after those for J_{NPF}.

The number concentration in the Aitken mode was generally considerably greater than that in the accumulation mode, whereas the concentrations of surface area and volume (and thus mass) in the accumulation mode were considerably greater than those in the Aitken mode. V_{ATK} exhibited much less variation among NPF formulations than did N_{ATK}, as new particles, because of their size, contribute little to volume concentrations in that mode. N_{ACC} was nearly independent of NPF formulation in most instances, implying that its major source was emissions. The main removal process of N_{ACC} was wet deposition, as shown by sharp decreases in N_{ACC} coincident with precipitation events.

For each NPF formulation $D_{\mathrm{g,ATK}}$ typically exhibited a diurnal variation opposite of that of J_{NPF} (Fig. 5), decreasing as new 3 nm particles were formed during the daytime and increasing because of coagulation at night. When appreciable NPF occurred, $D_{\mathrm{g,ATK}}$ at the lowest model level was the smallest (a few nm) at local noon and the largest (several tens of nm) at night. The lowest daytime $D_{\mathrm{g,ATK}}$ generally occurred for THN but the greatest occurred, unexpectedly, for BHNJ. This was attributed to NPF occurring at higher altitudes (cf. Fig. 6), with new particles being rapidly transported to the surface where they underwent growth by condensation and coagulation. This inference is supported by the finding that large values of $D_{\mathrm{g,ATK}}$ were accompanied by high self-coagulation rates and high sulfate concentrations in the Aitken mode, e.g. on 3 July at Site A (Fig. 5a). In contrast to $D_{\mathrm{g,ATK}}$, there was very little temporal variation of $D_{\mathrm{g,ACC}}$, this quantity being near 70 nm (corresponding to the geometric mean dry diameter of the number size distribution of emissions, as noted above) at each site, independent of NPF formulation, except for abrupt decreases coincident with precipitation events (shown by occurrences of high wet deposition), in which larger particles are preferentially activated to form cloud drops and subsequently removed. This finding also suggests that the dominant source of accumulation mode particles was primary emissions.

When IMT occurred, it exhibited diurnal variation similar to that of J_{NPF}. However, the occurrence of IMT at the several sites was quite intermittent, being associated with NPF (no IMT occurred for the BASE case) but not occurring in all instances of NPF. The dependence of IMT on J_{NPF} and $[H_2SO_4]$ is examined in Fig. 7, which shows IMT fraction, the fraction of time intervals for which IMT occurred anywhere in the columns over the four sites (i.e., including all vertical layers) for the entire month of July. For low values of J_{NPF} (i.e., <10 cm^{-3} s^{-1}), IMT fraction is quite low (<15%) and exhibits a weak dependence on J_{NPF}, but this fraction increases strongly with increasing J_{NPF} for larger values, approaching 100% for $J_{NPF} = 10^3$ cm^{-3} s^{-1} (Fig. 7a). In contrast, IMT fraction is nearly independent of $[H_2SO_4]$ above a minimum value for J_{NPF} in the range 10-100 cm^{-3} s^{-1} (Fig. 7b).

Aitken and accumulation mode aerosol particles were typically composed mainly of sulfate and ammonium, the acidity of particles being determined by the availability of ammonia, which differed among the sites. In some instances there was an appreciable contribution from secondary organic aerosol, SOA, although this typically comprised at most a few percent of total particle mass in the Aitken and accumulation modes. SOA is reported as often constituting a substantial fraction of the mass of fine particles in the atmosphere (Saxena and Hildemann, 1996; Zhang et al., 2007), which would imply that the contribution of SOA to particle growth may be underestimated in the present model. However, as discussed below, this does not seem to always be the situation.

As expected, there were considerable differences in NPF between the sites. At Site A, a rural location, $[H_2SO_4]$ frequently exceeded 10^7 cm^{-3} near local noon and $[NH_3]$ was typically quite high. Under these conditions there were large differences in the frequency and rate of NPF between the different formulations, with THN exhibiting the highest rates of NPF, followed by EM97 and NIIR. The fraction of time intervals during which NPF occurred in the lowest model level at rates greater than 1 cm^{-3} s^{-1} was greatest for THN with 37% (out of 248 time intervals), followed by 29% for EM97 and only 1.6% for NIIR. NPF did not occur at all for BHNJ or BHNV, as the modeled $[H_2SO_4]$ was insufficient for NPF at the high temperatures at this location. THN frequently yielded rates of NPF that exceeded those typical of urban areas, ~100 cm^{-3} s^{-1} (Kulmala et al., 2004), and because the modeled $[NH_3]$ exceeded the parameterization limit given by Napari et al. (2002) of 100 ppt (above which the modeled J_{NPF} was held equal to the maximum given by the parameterization), the actual values of J and J_{NPF} may have even exceeded the values shown. These considerations suggest that J_{NPF} according to

THN exhibits high uncertainty in regions of high [NH_3]. Although BHNJ resulted in no NPF at the lowest model level, it yielded greater N_{ATK} than the BASE case did, suggesting rapid transport of new particles from above. The fraction of time intervals for which IMT occurred at the lowest level at Site A was 18% for THN but only 2.4% for EM97. NPF without IMT can occur because of the requirement for IMT that the condensational growth rate of aerosol mass in the Aitken mode must be greater than that in accumulation mode.

The concentrations of (dry) particle volume in the Aitken mode V_{ATK} at this site for THN, EM97, NIIR, and BHNJ were roughly the same, and they were typically greater than those in BASE and BHNV by an order of magnitude because of newly formed particles, which were too small to enhance V_{ATK} at their initial size, but which increased V_{ATK} by their further growth by condensation of substances (other than water) with rates constrained by available condensing vapor.

Although the time dependences of the various quantities of interest at Site B (Fig. 5b), semi-urban Connecticut, were similar to those at Site A, there were noticeable differences, especially in J_{NPF}, N_{ACC}, the occurrence of IMT, and $D_{\mathrm{g,ATK}}$. [H_2SO_4] was frequently greater than at Site A, and [NH_3] was typically considerably lower because of the molar mixing ratio of sulfate commonly exceeding half that of ammonium, resulting in unneutralized acid, e.g. July 3-5. Formulations exhibiting the greatest J_{NPF} and N_{ATK} were either THN, for which NPF was intermittent, or EM97. As for site A, BHN was not capable of NPF because the modeled [H_2SO_4] ($\leq 10^8$ cm^{-3}) was insufficient for NPF at this warmer location (T>290 K). The fraction of time intervals for which IMT occurred at the lowest model level for EM97 increased from 2.4% at Site A to 17% at Site B because the greater [H_2SO_4] resulted in greater J_{NPF} and consequently more frequent IMT according to this formulation. $D_{\mathrm{g,ATK}}$ was greater for THN than for EM97, and even the greatest among all NPF formulations considered in some instances, because the intermittent nature of NPF by this formulation allowed more time for new particles to grow by self-coagulation and condensation.

At Site C, the remote downwind site, [SO_2] and [NH_3] were generally considerably lower (Fig. 5c) than at sites A and B. Some instances of high values occurred, but these can be attributed to transport from different locations. Insight into the origins of SO_2 and NH_3 can be found in maps of emissions of these substances (Fig. 3); strong sources of SO_2 lie south of this site, whereas strong sources of NH_3 lie both north and south of this site. During transit NH_3 would be consumed to neutralize H_2SO_4, indicating that instances of simultaneous high $[H_2SO_4]$ and $[NH_3]$ would be rare at this site. In addition F_{KK} was typically low because $[H_2SO_4]$ was quite low despite low background aerosol concentration. Under these conditions NPF events were weaker and less frequent than at Site A or B, and, when they occurred, were mainly by THN in situations of northwesterly winds. On the other hand, the number of occurrences of IMT was not less than that at Site A or B, although the magnitude of such events generally was too small ($<10^{-3}$ cm^{-3} s^{-1}) to influence N_{ACC} appreciably. As the occurrence of IMT does not depend strongly on J_{NPF} when J_{NPF} is less than 10 cm^{-3} s^{-1} (Fig. 7a), most instances of IMT at this site could not be explained by local NPF and must therefore have involved Aitken particles brought to the site by either vertical or horizontal transport.

At Site D, the remote marine site, $[SO_2]$ and $[NH_3]$ were generally also considerably lower (Fig. 5d) than at sites A and B. $[H_2SO_4]$ exceeded 10^6 cm^{-3} only when the site was under the influence of transport from the adjacent continent. For example, on 10 July Site D was located under the east flank of a low pressure system which transported SO_2 leaving the continent at Delaware along 38º N under a strong southwesterly wind. The production of H_2SO_4 from local oxidation of SO_2 advected into this region resulted in a few significant NPF events, and only by EM97. NPF by THN did not occur because ammonia had been totally consumed to neutralize acidic species before leaving the continent, and NPF by BHNV or BHNJ did not occur in the lowest model level because of the high temperature there (T~290 K). However, events of NPF by EM97 were not accompanied by increases in concentrations of surface area or volume in the Aitken mode because of insufficient condensable vapor; consequently EM97 had the lowest $D_{g,ATK}$ among all model variants. $D_{g,ATK}$ was typically higher for the BASE case, as no IMT occurred and particles continued to grow without being removed from the Aitken mode. Omission of sea salt and DMS emissions in the model would be expected to impact this site more than any of the others. The main consequence of sea salt would have been a greater condensational sink; however, as concentrations of condensable vapor at this site were often low (Fig. 5d), the consequences of not including sea salt were probably minor. DMS through its oxidation would result in SO_2, and through its oxidation H_2SO_4, suggesting that concentrations of these substances may have been underestimated, but the air mass at this location was certainly strongly continentally influenced (Fig. 3) with relatively little time spent over the water for oxidation to occur, so the consequences of not including DMS are probably minor as well.

An attempt was made to evaluate the representativeness of mixing ratios of SO_2 used in calculation of the H_2SO_4 production rate by comparison with measurements made at nearby U. S. Environmental Protection Agency air quality monitoring stations for the several locations examined in Fig. 5. Such evaluations are particularly difficult for a primary emittant such as SO_2, which derives mainly from point sources and which consequently exhibits considerable short-term and subgrid variability relative to calculations obtained with a continental scale model such as employed here. A further limitation on such comparisons is the tendency to locate SO_2 monitoring stations in the vicinity of sources in order to ascertain compliance with air quality standards. The consequences of such considerations are shown in the panel for site B (Fig. 5b), which shows observed SO_2 mixing ratios from two monitoring sites, one at the New Haven-Meriden, Connecticut site, 25 km from site B, and one at the Waterbury, Connecticut site, 50 km from site B (and 30 km from the Meriden site). The SO_2 mixing ratio at the New Haven-Meriden site exhibited rather large excursions and rather high values compared to the Waterbury site, which appears to be more regionally representative and at which mixing ratios were much suitable for comparison with the model calculations. A similar situation obtained for site C, coastal Maine, for which the proximate sites exhibited highly varying temporal profiles of SO_2 (Fig. 5c); for example the Oxford, Maine site, ~225 km from site C, showed magnitudes closer to those obtained in the present calculations than did the more urban Portland, Maine site ~175 km from site C (and 100 km from the Oxford site). For site A the only proximate stations, one in nearby Sioux Falls, South Dakota, 40 km from site A, and the other in Mason City, Iowa, ~250 km from site A, again exhibited rather differing SO_2 profiles (not shown). In summary the limited available comparisons suggest that the SO_2 mixing ratios obtained from the model and used in calculation of H_2SO_4 production rate are regionally representative.

Examination of vertical profiles of NPF-related variables yields insight into the dependence of key processes on altitude and the role of vertical mixing. Vertical profiles of $[H_2SO_4]$, $[NH_3]$, T, RH, J_{NPF}, N_{ATK} and $D_{\mathrm{g,ATK}}$ at local noon averaged for July at Site B (which is at sea level) are shown for the different model variants in Fig. 6. Sulfuric acid was formed at substantial concentrations up to 5 km, whereas ammonia was primarily below 2 km. Air temperature decreased monotonically to less than -40°C near the tropopause (near 12 km), whereas RH peaked near the top of the planetary boundary layer (PBL) at ~1-1.5 km. Under these conditions, appreciable NPF occurred at heights up to 5 km for EM97 and NIIR, whereas it was confined to the PBL for THN. NPF from BHNJ occurred at heights of between 1 and 3 km following the behaviour of *RH*, and near the tropopause, whereas NPF from BHNV was negligible over the heights shown. N_{ATK} and $D_{\mathrm{g,ATK}}$ tended to be rather uniform throughout the PBL for several of the formulations, including BHNJ, for which there was little production at the surface, implying that substantial vertical mixing occurred within the PBL.

The influence of the several NPF formulations on J_{NPF} and N_{ATK} is examined as a function of location over the entire continental U.S. in Fig. 8, which shows the averages of these quantities over the PBL and over the free troposphere (FT). The dissimilar spatial distribution of J_{NPF} for different NPF formulations is attributed mainly to the spatial distribution of NPF precursors, NH_3 and H_2SO_4. Despite ammonia emissions being greatest over the middle and eastern U.S. (Fig. 3), [NH_3] was lower in the eastern U.S. than in the western U.S. because of neutralization by sulfuric acid. In the western U.S., because of lower emission of SO_2 (Fig. 3), much ammonia remained in the gas phase, allowing NPF by THN. As production of H_2SO_4 required time for the photochemical reaction, NPF by the EM97 and NIIR formulations were somewhat displaced from sources of SO_2, which were mostly located over eastern U.S. Because SO_2 has a longer residence time than NH_3, EM97 and NIIR resulted in more widespread distributions of NPF than did THN, but at a lower rate. Widespread NPF events have been observed at a variety of places in the U.S. (for comprehensive reviews see Kulmala et al., 2004 and Yu et al., 2008), including locations that are rural (Idaho Hill, Colorado, Marti et al., 1997), coastal (Washington state coast, Hegg et al., 1992), and urban (e.g., Atlanta, Georgia, Woo et al., 2001, Stolzenburg et al., 2005; Pittsburgh, Stanier et al., 2004). Although the fundamental mechanism explaining the ubiquitous background of ultrafine aerosols in the atmosphere remains poorly understood, examination of Fig. 8 suggests that it might be better accounted for by superposition of several NPF mechanisms rather than by a single mechanism.

3.2 Sensitivity to primary emissions

The sensitivities of modeled number concentrations and other aerosol properties to sizes (numbers) of emitted particles were examined by analyzing model results for the lowest level at site B for three cases. In the D_0 case, the geometric mean diameters of emitted particle mass for the Aitken and accumulation modes ($D_{g,ATK}$ and $D_{g,ACC}$, respectively) retain their initial values of 30 nm and 300 nm, respectively. In the $D/2$ case, $D_{g,ATK}$ and $D_{g,ACC}$ were decreased to 15 nm and 150 nm, respectively, and in the $D\times2$ case, $D_{g,ATK}$ and $D_{g,ACC}$ were increased from their initial values to 60 nm and 600 nm, respectively, while in both of the latter two cases the total emitted mass was held constant and distributed as noted above, with 99.9% going into the accumulation mode and 0.1% into the Aitken mode. Here examination was restricted to NPF occurring jointly by both the THN and the NIIR formulations (THN+NIIR). Time series of [H_2SO_4], J_{NPF}, number concentrations in the Aitken and accumulation modes, and other related quantities for each case at the lowest model level at Site B are shown in Fig. 9.

A decrease (increase) in particle diameter by a factor of 2, for constant mass emissions, results in an increase (decrease) in the number of emitted particles by a factor of 8, and an increase (decrease) in the total concentration of surface area of emitted particles by a factor of 2; lines denoting these factors are shown in Fig. 9. Associated with the increase (decrease) in surface area concentration would be a nearly proportional increase (decrease) in rate of condensation were no other factors at play. The situation with coagulation is more involved, as the rate of coagulation of particles of two diameters is directly proportional to the product of their number concentrations, the sum of their diameters, and the sum of their diffusion coefficients (each of which is inversely proportional to the square of the particle diameter for particles with diameters appreciably less than the mean free path of air, ~65 nm at sea level, and inversely proportional to the particle diameter for appreciably larger particles). If no other processes acted, a decrease (increase) in particle diameter by a factor of 2, for constant mass emissions, would result in an increase (decrease) in the first factor by 64 ($=8^2$), in the next by 1/2, and in the third by 4 for self-coagulation of Aitken mode particles, resulting in an increase (decrease) of 128. The increase (decrease) for the self-coagulation rate of accumulation mode particles would be somewhat less because of their larger size and weaker dependence of diffusion coefficient on particle size. Lines denoting a factor of 128 in the self-coagulation rate for the Aitken and accumulation modes are also shown in Fig. 9.

Not surprisingly, the $D/2$ case systematically resulted in an increase, and the $D\times2$ case in a decrease, in N_{ACC} (Fig. 9), indicating that this quantity is largely determined by primary emissions. However, the increase (decrease) in N_{ACC} was typically about a factor of 4, and the decrease (increase) in $D_{\mathrm{g,ACC}}$ was slightly less than a factor of 2—less than what would have resulted if the number concentration were controlled entirely by primary emission and no coagulation occurred (a factor of 8 for N_{ACC} and a factor of 2 for $D_{\mathrm{g,ACC}}$). The quantities $[\mathrm{SO_4}]_{\mathrm{ACC}}$, $[\mathrm{NH_4}]_{\mathrm{ACC}}$, and $[\mathrm{SOA}]_{\mathrm{ACC}}$ were nearly the same for each case at almost all times, although in some instances (e.g., 21 July) $[\mathrm{SO_4}^{2-}]_{\mathrm{ACC}}$ and $[\mathrm{NH_4}^{+}]_{\mathrm{ACC}}$ were slightly greater for the $D/2$ case and slightly less for the $D\times2$ case than for the D_0 case, reflecting the increased (decreased) rate of condensation associated with the increased (decreased) surface area concentration accompanying the decrease (increase) in size of emitted particles. Additionally, there was a nearly uniform increase (decrease) in the self-coagulation rate of accumulation mode particles by roughly a factor of 50 accompanying the decrease (increase) in the diameter of emitted particles. As expected, the rate of wet deposition of accumulation mode particles was greatest for the $D/2$ case, reflecting the greater number of particles available to be removed by precipitation.

In contrast to these results, N_{ATK} was generally less for the $D/2$ case, and slightly greater for the $D\times2$ case, than for the D_0 case (Fig. 9), implying that primary emissions were not a dominant factor in controlling N_{ATK}. Additionally, $D_{\mathrm{g,ATK}}$ was often less for the $D/2$ case than for the D_0 case, but it was nearly the same for the $D\times2$ and D_0 cases. These results can be explained by suppression of NPF by the greater condensational sink (in both modes) for $\mathrm{H_2SO_4}$ accompanying the decrease in size of emitted particles (i.e., $D/2$ case), resulting in a decrease in $[\mathrm{H_2SO_4}]$, this increased condensation sink and consequent decrease in $[\mathrm{H_2SO_4}]$ providing less favorable conditions for NPF. For example, $D_{\mathrm{g,ATK}}$ was the greatest in the $D\times2$ case on 12 July (green circle in Fig. 9) when $J_{\mathrm{NPF}} < 10^{-3}\ \mathrm{cm^{-3}\ s^{-1}}$, whereas $D_{\mathrm{g,ATK}}$ was the smallest in the same case on 15 July (brown circle in Fig. 9) when $J_{\mathrm{NPF}} > 10^{2}\ \mathrm{cm^{-3}\ s^{-1}}$. In support of this explanation, there were sometimes large differences in J_{NPF} between the several cases with less NPF typically occurring for the $D/2$ case than for the other two cases. Also, F_{KK} was often greater for the $D\times2$ case than for the others, and there were several instances in which IMT occurred for the $D\times2$ case but not either of the others. These findings support the conclusion that N_{ATK} is determined much more by

NPF than by primary emissions. Also consistent with this explanation is the typically greater rate of self-coagulation in the Aitken mode in the $D\times2$ case than in the $D/2$ case. $[SO_4]_{ATK}$ and $[NH_4]_{ATK}$ were occasionally greater for $D\times2$ case, although they were often independent of case. The dry deposition flux of Aitken mode particle number, for which the strong peaks tend to accompany large values of N_{ATK}, was also nearly independent of case.

3.3 Budgets of aerosol number concentration

The factors controlling aerosol number concentrations in the Aitken and accumulation modes are further examined by consideration of the number budget, i.e., the magnitudes of the various sources and sink rates of aerosol number concentration, in both modes, averaged over the entire modeling domain and time for each model variant (Fig. 10). The overwhelmingly dominant source of number concentration in the Aitken mode was NPF, which greatly exceeded primary emissions in all model variants (except the BASE case, for which there was no NPF); consequently, N_{ATK} is insensitive to the specific fraction of mass assumed to be emitted into the Aitken mode, here taken as 0.1%. The main sink of number concentration in the Aitken mode was coagulation, with minor contributions from wet and dry deposition. IMT was generally negligible, being no more than a few percent of coagulation for BHNJ, and even less for other model variants. Although J_{NPF} differed by more than three orders of magnitude among the several NPF formulations (Fig. 10), the resulting N_{ATK} exhibited a range of only about two orders of magnitude (Table 2), the smaller range being attributed to increased coagulation of the very small particles resulting from larger values of J_{NPF}. The turnover time for particle number in the Aitken mode, $\tau_{N,ATK}$, defined as the total number of Aitken mode particles in the domain divided by the total loss rate due to physical processes (i.e., not including transport in and out of the domain), ranged from 0.03 d to 0.5 d among the five NPF formulations (Table 2), being determined largely by the coagulation rate. The smallest turnover times occurred for THN and THN+NIIR (i.e., D_0, $D\times2$, and $D/2$), as these resulted in the largest values of N_{ATK}, and thus even greater coagulation rates, which are directly proportional to the squares of the number concentrations.

The dominant source of aerosol number concentration in the accumulation mode was primary emission, although for some model variants IMT provided a nearly equal contribution

(Fig. 10). Thus, the largest variation of N_{ACC} occurred by altering the size of emitted particles (Table 2). As IMT introduced particles into the accumulation mode at small sizes, the overwhelming contribution to the mass concentration in this mode was provided by emissions. The dominant sink of number concentration in this mode was wet deposition (including removal of unactivated particles by coagulation on activated accumulation mode particles), which was nearly the same for all model variants except the $D/2$ case, with coagulation generally providing a relatively minor contribution, which was also roughly the same for all model variants except the $D/2$ case. For the $D/2$ case both contributions were nearly equal to each other and greater than for the other model variants. In this case the initial particles were smaller and IMT resulted in more and smaller particles in this mode. The contribution from dry deposition was generally negligible for all model variants. Consequently, the turnover time for particle number in the accumulation mode, $\tau_{\mathrm{N,ACC}}$, was nearly independent of model variant at around 2.7 d, except for the $D/2$ case when it was 1.6 d because of the increased loss of particle number due to coagulation (Table 2).

The mean turnover time for aerosol mass, which resides almost entirely in the accumulation mode (Fig. 5), is defined similarly to that for aerosol number, although loss mechanisms differ. Importantly, coagulation results in a loss of number but leaves mass unchanged; thus, only wet and dry deposition act as sinks for aerosol mass. However, the importance of these processes differs between mass and number concentrations, as they affect particles of different sizes differently. The turnover time for total aerosol mass was ~8 d for all model variants in the present study, characteristic of the time between precipitation events (Fig. 5). This time is greater than that for aerosol number, for which coagulation is also a sink, and is comparable to that of sulfate mass reported in several other model studies (e.g., 6.5 d by Adams and Seinfeld, 2002, and 7.0 d by Benkovitz et al., 2004), although it is considerably greater than the mean of 4.1±0.7 d for 15 studies reviewed by Textor et al. (2006). The longer turnover time found here compared to those studies is attributed to the paucity of precipitation events in the model domain during July, 2004.

4 Comparison with Observations

Model results were compared with aircraft measurements taken over the northeast U.S. and eastern Canada using the NOAA (National Oceanographic and Atmospheric Administration) WP-3D (P3) aircraft during the ICARTT 2004 study (Fehsenfeld et al., 2006, Nowak et al., 2007). Tracks of the flights used in the present comparisons are shown in Fig. 11 and are seen to include sites B, C, and D. For each observational data point shown in Figure 12, data from the eight nearest grid-cell midpoints to the location of the P3 were sampled and then bi-linearly interpolated to the location of the aircraft. Model calculations of number, surface area, and volume concentrations for the Aitken and accumulation modes for the several NPF formulations were summed and compared to the integrals of the aircraft measurements for (dry) diameters from 3 nm to 2.5 μm. Although the number concentration was dominated by the Aitken mode, the main contributions to the concentrations of surface area and volume were from the accumulation mode. The different NPF formulations differed primarily in number concentrations, and exhibited nearly the same concentrations of surface area and volume, similar to the situation with the model results at the different sites at ground level (Fig. 5).

In some instances the model did poorly (some of these are shown as orange bands in Fig. 12), especially at higher altitude and during the ascent and descent of the aircraft. There seem to be several reasons for the poor performance. For example, on 9 July the aircraft encountered a biomass-burning plume at 4 km, which is thought to have come from Canadian and Alaskan forest fires (Fehsenfeld et al., 2006); the wind in both observation and model was from the north where no Canadian area sources were taken into account. The sharp peaks in surface area and volume concentrations observed at height 3 km from 17:00 to 18:00 UST on 20 July came from a biomass-burning plume (Fehsenfeld et al., 2006) which was not captured by the model. A biomass-burning plume was also encountered on 28 July (Fehsenfeld et al., 2006). High surface area and volume concentrations in the lower marine atmosphere (61°W, 40.5°N) between 15:00 and 16:00 UTC on 15 July may have been due to the presence of sea salt particles, emission of which was not treated in the model. The modeled wind speed was relatively high (~8 m s^{-1} at 7 m) because the area was under the influence of a cyclonic low pressure system, and production of sea salt particles would thus be expected. There were probably other factors that also contributed, as at times immediately following these the concentrations of surface area and volume simulated by the model agreed fairly well with observations although the number concentrations were underestimated by nearly an order of magnitude.

In general, however, the model did rather well in reproducing aerosol concentrations, especially at lower altitudes (some instances are denoted by brown circles in Fig. 12). For example, the rather fresh Boston plume on 9 July around 18:00 UTC was captured by the model, as was a well defined New York City plume on 15 July from 18:00 to 21:00 UTC (Fehsenfeld et al., 2006). In addition, the high values of the number, surface area, and volume concentrations observed on 20 July, reaching up to 2 km, were well matched by the modeled ones through all heights. The model also performed well on 25 and 27 July. Among the several NPF formulations considered EM97 reproduced number concentration best, but agreement was good only at lower altitudes.

A substantial fraction of the differences between model and observation may be due to subgrid variation (Benkovitz et al., 2004). The effect of subgrid variation was examined by comparing results from the two different model resolutions, 60 km with 3 h output and 12 km with 10 min output, both using the sum of the THN and NIIR formulations, with P3 measurements taken on 20 July (Fig. 13). For most of the quantities compared the results from the two resolutions were quite similar, and for some quantities they agreed rather well with the observations. Modeled values of $[SO_4^{2-}]$ were greater than observations, but the 12-km resolution version of the model generally provided greater accuracy, as it did also for $[NO_3^-]$. The high temporal variability of modeled $[NO_3^-]$ between 14:30 and 15:00 UTC in the 60-km resolution version of the model may be due to sampling model data from the edge of the modeled plume centered at 72°W and 39°N (not shown here). Both resolutions underestimated $[NH_3]$, but as $[NH_3]$ is, to good approximation, equal to the difference (in equivalent units) between total [N(-III)] (the sum of $[NH_3]$ and $[NH_4^+]$) and the sum of $[SO_4^{2-}]$ and $[NO_3^-]$, underestimation of $[NH_3]$ is mainly a consequence of the overestimation of sulfate, which occurs in both model resolutions (although considerably less so in the higher resolution model). The low-biased $[NH_3]$ may be the reason that the model underpredicted aerosol number concentration, exhibiting much lower concentrations of small particles (bottom three panels) between 16:30 and 17:00 UTC and between 18:00 and 19:30 UTC than those measured, which attain values up to near $2 \cdot 10^4$ cm^{-3}. Concentrations of number, surface area, and volume were often underestimated by both model resolutions, although in some instances (e.g., 19:30-20:00 UTC) the 12 km model overpredicted number concentration but underpredicted surface area and volume concentrations. One interesting feature of the comparisons is the relatively good agreement between measured and modeled SOA, implying that it might not be underestimated in models as suggested by some investigators.

5 Summary and Conclusions

The dependence of aerosol number concentration and other intensive and extensive aerosol properties on different formulations of new particle formation NPF and on the particle size and number of primary emissions has been examined using the regional CMAQ model over the continental U.S. for July 2004. The calculated rate of NPF, J_{NPF}, varied greatly for the several NPF formulations examined, and for any given NPF formulation J_{NPF} varied greatly in time and space. Because of the relatively high ammonia concentration in the western U.S. compared to the eastern U.S., where high SO_2 emissions and resultant high sulfate concentrations result in low NH_3 concentrations, ternary homogeneous nucleation (THN) involving ammonia together with sulfuric acid and water was the dominant NPF mechanism in the western U.S. In the eastern U.S. J_{NPF} was greatest for the empirical formulation of Eisele and McMurry (1997). New particle formation by ion-ion recombination (NIIR) provided a substantial contribution across the whole domain; however, recent field studies showing that ion-induced nucleation is insignificant compared to other mechanisms of NPF (Eisele et al., 2006; Iida et al, 2006) suggest that the NIIR formulation employed here may substantially overestimate J_{NPF} by that mechanism. NPF by THN and by NIIR occurred primarily in the planetary boundary layer, whereas for both binary (sulfuric acid and water) homogenous nucleation formulations considered NPF occurred primarily near the tropopause because of the low temperature there, but at a relatively low rate.

For each NPF formulation considered the major source of aerosol number concentration in the Aitken mode was NPF despite the large variation in J_{NPF} among the several formulations, with the contribution from emissions being considerably less. The major source of domain-average aerosol number concentration in the accumulation mode was primary emission, but for instances of intense NPF a comparable source was provided by transfer of Aitken mode particles to the accumulation mode, although this process contributed very little to the accumulation mode mass concentration. When NPF occurred, the characteristic diameter of Aitken mode particles $D_{\mathrm{g,ATK}}$ exhibited a diurnal variation opposite to that of J_{NPF} because NPF reduced $D_{\mathrm{g,ATK}}$, whereas subsequent coagulation increased $D_{\mathrm{g,ATK}}$ to near its previous value. In contrast, the characteristic diameter of accumulation mode particles $D_{g,ACC}$ exhibited little dependence on NPF formulation, being controlled mainly by the diameter of emitted particles.

The sensitivity of aerosol properties to change in size of emitted particles for constant mass emission rate was examined, a factor of 2 decrease (increase) in particle size resulting in a factor of 8 increase (decrease) in number emission rate. Surprisingly, it was found that an increase (decrease) in the number of emitted particles resulted in a decrease (increase) in the number concentration of Aitken mode particles N_{ATK}. This is attributed to NPF being controlled by sulfuric acid vapor; when the size of emitted particles is decreased, the resultant increase in surface area increases the sink rate of sulfuric acid vapor, suppressing NPF and resulting in an overall decrease in N_{ATK}. In contrast, the dominant sensitivity of the number concentration of accumulation mode particles N_{ACC} is to the size (number) of the emitted particles (for constant mass emissions). The change in N_{ACC} in response to changes in number and size of emitted particles was in the direction expected, but at a somewhat lower magnitude (roughly a factor of 4) than would be expected (a factor of 8) if primary emitted particles were the only source of accumulation mode particles and no coagulation occurred.

The sensitivity of N_{ACC} to NPF formulation and to the size (number) of emitted primary particles would result in a high uncertainty in the calculation of aerosol indirect effects, which depend on aerosol number concentration. In this context, it might be noted that an increase of only 30% in droplet number concentration in marine stratus clouds globally corresponds to a climate forcing of 1 W m^{-2} (Charlson et al., 1992). The present study thus demonstrates the need for both NPF and primary emissions to be better constrained if the direct and first indirect effects are to be accurately represented in models of aerosol forcing and ultimately in climate models.

Comparison of model results to measurements yielded many instances of rather good performance of the model for surface area and volume, especially in the planetary boundary layer, where emissions were mainly within the model domain. However, in the free troposphere the model accuracy was often less; this is attributed to missing sources of particles and/or long-range transport from outside the model domain. This finding suggests the need for addition of biomass burning sources and for more realistic boundary conditions for regional scale models, or perhaps extension of the model domain to a larger scale; the need to include the entire northern hemisphere in modeling sulfate aerosol mass concentration has been noted previously

(Benkovitz et al., 2004). Chemical composition and number concentrations obtained from the 12-km resolution version of the model were closer to measurements than were those obtained from the 60-km resolution version.

The main limitations of this model, which might affect the analysis of the consequences of different treatments of NPF and emissions, are the modal framework (specifically the constrained aerosol evolution resulting from the assumption of lognormal size distributions and the artificial intermodal transfer from the Aitken mode to the accumulation mode), inaccuracy in the conversion factor from nuclei to new particles due to neglect of self-coagulation, uncertainty in the size of emitted primary particles, and lack of emissions of aerosol species such as sea salt and biomass burning. A potential concern with the modal method as applied here is the inclusion of newly formed particles in the Aitken mode and the potential resultant broadening of this mode. Although another mode containing newly formed particles might be added, this approach would necessitate deciding when sufficient new particle formulation occurred to introduce this mode, establishing criteria for intermodal transfer between this new particle mode and the Aitken mode, and the like. In any event, as the modeled geometric standard deviation of the Aitken mode σ_{ATK} exhibited values between ~1.4 and 2.1, rarely exceeding 2.0, such broadening would seem to be of minimal concern.

While this study points to and quantifies some of the consequences that result from differing assumptions on NPF formulation and on primary emissions, model studies such as this can at best determine only the consequences of the assumptions that are coded in the model. Resolution of the large differences in number concentration revealed here for different model variants ultimately rests on measurements. In that respect we note the dearth of measurements characterizing size distributions (and even more so, size-distributed composition) of primary particulate matter from the many processes that give rise to such emissions. Characterization of particulate emissions has focused almost entirely on mass emission rates, this focus arising from air quality considerations and standards that are prescribed in terms of mass concentrations of particulate matter with (aerodynamic) diameter (at a given RH) less than a given value, e.g., 2.5 μm or 10 μm in the United States. Consequently assumptions such as that made here that 99.9% of the emitted mass is in the accumulation mode and only 0.1% is in the Aitken mode, have little support in measurement (although the results of this investigation suggest that the specific fraction of mass assumed to be emitted into the Aitken mode has little effect on N_{ATK}). Likewise, NPF rates and their dependence on controlling variables are highly uncertain, and even the mechanisms involved are not completely understood. Here we treated only NPF involving sulfuric acid, ammonia, and water vapor, which have been thought to be the major contributors to NPF in the atmosphere and consequently received considerable attention. However, evidence is becoming available from measurements that organic substances can also participate in NPF. For example, measurements of the composition of newly formed particles with diameter as low as 10 nm in Mexico City (Smith et al., 2008) have shown that these particles may contain an order of magnitude more organics than sulfates, with growth rate based on measured sulfuric acid concentration being an order of magnitude less than the observed growth rate. Additionally, parameterizations for NPF rates are being updated on the basis of new studies and as other mechanisms are considered. For instance, recent investigations (Kuang et al., 2008) suggest that the exponent p in Eq. (3) denoting the power law dependence of nucleation rate on sulfuric acid concentration is equal to 2 to within experimental uncertainty, and that the value of K used in this equation (denoting the magnitude of the rate) is typically greater than that used in the model by more than an order of magnitude. An updated formulation of ternary homogeneous nucleation of sulfuric acid, ammonia, and water (Merikanto et al., 2007) that includes presumed effects of stable ammonium bisulfate (despite absence of experimental evidence for the presence of this substance) yields nucleation rates several orders of magnitude lower than those of Napari et al. (2002). A new formulation for the fraction of stable nuclei that grow to become new particles, the quantity F_{KK} in Eq. (2), was recently presented by Lehtinen et al. (2007); however, there remains much uncertainty in this fraction, and the assumptions required for its computation, that the growth rate and condensation sink remain constant during a time step, and that self-coagulation of nuclei smaller than new particles does not occur, preclude the possibility of the model capturing an extremely strong pulse-type nucleation that is self-quenching. Confident representation of the responsible processes in models, and the dependence on controlling variables—concentrations of precursor gases, insolation, and the like—requires determination of these dependences in laboratory studies and confirmation of these mechanisms by field measurements.

Acknowledgments

This work was supported by the U.S. Department of Energy's Atmospheric Science Program (Office of Science, OBER) under Contract No. DE-AC02-98CH10886. We acknowledge Douglas L. Wright of Rutgers University for his early work on this study. We thank Stuart McKeen (NOAA) for providing emission data, Gregory R. Carmichael (University of Iowa) for providing meteorological data, Charles Brock (NOAA) for providing aerosol number distribution data, John Nowak (NOAA) for providing ammonia data, and Ann Middlebrook (NOAA) for providing aerosol mass spectrometer data.

References

Adams, P. J., and J. H. Seinfeld (2002), Predicting global aerosol size distributions in general circulation models, *J. Geophys. Res.*, 107, doi:10.1029/2001JD001010.

Adams, P. J., and J. H. Seinfeld (2003), Disproportionate impact of particulate emissions on global cloud condensation nuclei concentrations, *Geophys. Res. Letts.*, 30(5), 1239, doi:10.1029/2002GL016303.

Benkovitz, C. M., S. E. Schwartz, M. P. Jensen, M. A. Miller, R. C. Easter, and T. S. Bates (2004), Modeling atmospheric sulfur over the Northern Hemisphere during the Aerosol Characterization Experiment 2 experimental period, *J. Geophys. Res.*, 109, D22207, doi:10.1029/2004JD004939.

Binkowski, F. S. (1999), Aerosols in models-3 CMAQ. Chap. 10, *Science Algorithms of the EPA Models-3 Community Multiscale Air Quality (CMAQ) Modeling System*, eds. Byun, D. W. and Ching, J. K. S. EPA/600/R-99/030, National Exposure Research Laboratory, Research Triangle Park, NC.

Binkowski, F. S., and S. J. Roselle (2003), Models-3 Community Multiscale Air Quality (CMAQ) model aerosol component I. Model description, *J. Geophys. Res.*, 108, D64183, doi:10.1029/2001JD001409.

Boucher, O., and U. Lohmann (1995), The sulfate-CCN-cloud albedo effect, *Tellus*, B47, 281-300.

Byun, D. W., and J. K. S. Ching, eds. (1999), *Science Algorithms of the EPA Models-3 Community Multiscale Air Quality (CMAQ) Modeling System*, EPA/600/R-99/030, National Exposure Research Laboratory, Research Triangle Park, NC.

Byun D. W., J. E. Pleim, R. T. Tang, and A. Bourgeois, A. (1999), Meteorology-chemistry interface processor (MCIP) for Models-3 Community Multiscale Air Quality (CMAQ) modeling system, Chap. 12, *Science Algorithms of the EPA Models-3 Community Multiscale Air Quality (CMAQ) Modeling System*, eds. Byun, D. W. and J. K. S. Ching, EPA/600/R-99/030, National Exposure Research Laboratory, Research Triangle Park, NC.

Carter, W. P. L. (2000), Implementation of the SAPRC-99 chemical mechanism into the models-3 framework, Report to the United States Environmental Protection Agency, January 29, 2000. Available at http://www.cert.ucr.edu/~carter/absts.htm#s99mod3.

Chang, J. R., R. A. Brost, I. S. A. Isaksen, S. Madronich, P. Middleton, W. R. Stockwell, and C. J. Walcek (1987), A three-dimensional Eulerian acid deposition model: Physical concepts and formulation, *J. Geophys. Res.*, 92(D12), 14681-14700.

Charlson, R. J., S. E. Schwartz, J. M. Hales, R. D. Cess, J. A. Coakley, Jr., J. E. Hansen, and D. J. Hofmann (2005), Climate forcing by anthropogenic aerosols, *Science*, 255, 423-430.

Chen, Y., and J. E. Penner (2005), Uncertainty analysis for estimates of the first indirect aerosol effect, *Atmos. Chem. Phys.*, 5, 2935-2948.

Dudhia, J. (1993), A nonhydrostatic version of the Penn State-NCAR mesoscale model: Validation tests and simulation of an Atlantic cyclone and cold front, *Mon. Weather Rev.*, 121, 1493-1513.

Eisele, F. L., and P. H. McMurry (1997), Recent progress in understanding particle nucleation and growth, *Phil. Trans. R. Soc. Lond.*, B352, 191-201.

Eisele, F. L., E. R. Lovejoy, E. Kosciuch, K. F. Moore, R. L. Mauldin, J. N. Smith, P. H. McMurry, and K. Iida (2006), Negative atmospheric ions and their potential role in ion-induced nucleation, *J. Geophys. Res.*, 111(D4), D04305: doi:10.1029/2005JD006568.

Fehsenfeld, F. C., G. Ancellet, T. S. Bates, A. H. Goldstein, R. M. Hardesty, R. Honrath, K. S. Law, A. C. Lewis, R. Leaitch, S. McKeen, J. Meagher, D. D. Parrish, A. A. P. Pszenny, P. B. Russell, J. Schlager, J. Seinfeld, R. Talbot, and R. Zbinden (2006), International Consortium for Atmospheric Research on Transport and Transformation (ICARTT): North America to Europe–Overview of the 2004 summer field study, *J. Geophys. Res.*, 111, D23S01, doi:10.1029/2006JD007829.

Ghan, S. J., R. C. Easter, E. G. Chapman, H. Abudul-Razzak, Y. Zhang, L. R. Leung, N. S. Laulainen, R. D. Saylor, and R. A. Zaveri (2001), A physically based estimate of radiative forcing by anthropogenic sulfate aerosol, *J. Geophys. Res.*, 106, 5279-5293.

Ghan, S. J., and S. E. Schwartz (2007), Aerosol properties and processes: A path from field and laboratory measurements to global climate models. *Bull. Amer. Met. Soc.*, 88, 1059-1083, doi:10.1175/BAMS-88-7-1059.

Hegg, D. A., D. S. Covert, and V. N.Kapustin (1992), Modeling a case of particle nucleation in the marine boundary layer, *J. Geophys. Res.*, 97(D9), 9851-9857.

Iida, K., M. Stolzenburg, P. McMurry, M. J. Dunn, J. N. Smith, F. Eisele, and P. Keady (2006), Contribution of ion-induced nucleation to new particle formation: Methodology and its application to atmospheric observations in Boulder, Colorado, *J. Geophys. Res.*, 111, D23201, doi:10.1029/2006JD007167.

Intergovernmental Panel on Climatic Chang (IPCC) (2007), *Climate Change 2007*: *Physical Science Basis*, ed. Solomon, S. et al., Cambridge Univ. Press.

Jaecker-Voirol, A., and P. Mirabel (1989), Heteromolecular nucleation in the sulfuric acid-water system, *Atmos. Environ.*, 23(9), 2053-2057.

Kerminen, V.-M., and M. Kulmala (2002), Analytical formulae connecting the "real" and the "apparent" nucleation rate and the nuclei number concentration for atmospheric nucleation events, *J. Aerosol Sci.*, 33, 609-622.

Kiehl, J. T., T. L. Schneider, P. J. Rasch, M. C. Barth, and J. Wong (2000), Radiative forcing due to sulfate aerosols from simulations with the National Center for Atmospheric Research Community Climate Model, Version 3, *J. Geophys. Res.*, 105, 1441-1457.

Kuang, C., P. H. McMurry, A. V. McCormick, and F. L. Eisele (2008), Dependence of nucleation rates on sulfuric acid vapor concentrations in diverse atmospheric locations, *J. Geophys. Res.*, 113, D10209, doi:10.1029/2007JD009253.

Kulmala, M., H. Vehkamäki, T. Petäjä, M. Dal Maso, A. Lauri, V.-M. Kerminen, W. Birmili, and P. H. McMurry (2004), Formation and growth rates of ultrafine atmospheric particles: a review of observations, *J. Aerosol Sci.*, 35, 143-176.

Lehtinen, K. E. J., M. K. Maso, M. Kulmala, and V.-M. Kerminen (2007), Estimating nucleation rates from apparent particle formation rates and vice versa: Revised formulation of the Kerminen-Kulmala equation, *J. Aerosol Sci.*, 38: 988-994.

Lucas, D. D., and H. Akimoto (2006), Evaluating aerosol nucleation parameterizations in a global atmospheric model, *Geophys. Res. Lett.*, 33, L10808, doi:10.1029/2006GL025672.

Marti, J. J., R. J. Weber, P. H. McMurry, F. Eisele, D. Tanner, and A. Jefferson (1997), New particle formation at a remote continental site: Assessing the contributions of SO2 and organic precursors. *J. Geophys. Res.*, 102D, 6331-6339.

McKeen, S., J. Wilczak, G. Grell, I. Djalalova, S. Peckham, E.-Y. Hsie, W. Gong, V. Bouchet, S. Menard, R. Moffet, J. McHenry, J. McQueen, Y. Tang, G. R. Carmichael, M. Pagowski, A. Chan, T. Dye, G. Frost, P. Lee, and R. Mathur (2005), Assessment of an ensemble of seven real-time ozone forecasts over eastern North America during the summer of 2004, *J. Geophys. Res.*, 110, D21307, doi: 10.1029/2005JD005858.

Menon, S., A. D. Del Genio, D. Koch, and G. Tselioudis (2002), GCM simulations of the aerosol indirect effect: sensitivity to cloud parameterization and aerosol burden, *J. Atmos. Sci.*, 59, 692-713.

Merikanto, J., I. Napari, H. Vehkamäki, T. Anttila, and M. Kulmala (2007), New parameterization of sulfuric acid-ammonia-water ternary nucleation rates at tropospheric conditions, *J. Geophys. Res.*, 112, D15207, doi:10.1029/2006JD007977.

Millikan, R. A., A. H. Neher, and W. H. Pickering (1944), Further studies on the origin of cosmic rays, *Phys. Rev.*, 66, 295-302.

Napari, I., M. Noppel, H. Vehkamäki, and M. Kulmala (2002), Parameterization of ternary nucleation rates for H_2SO_4-NH_3-H_2O vapors, *J. Geophys. Res.*, 107(D19), doi:10.1029/2002JD002132.

Neher, H, V. (1971), Cosmic rays at high latitudes and altitudes covering four solar maxima, *J. Geophys. Res.*, 76(7), 1637-1651.

Nenes, A., S. N. Pandis, and C. Pilinis (1998), ISORROPIA: A new thermodynamic equilibrium model for multiphase multicomponent inorganic aerosols, *Aquat. Geoch.*, 4, 123-152.

Nowak, J. B., J. A. Neuman, K. Kozai, L. G. Huey, D. J. Tanner, J. S. Holloway, T. B. Ryerson, G. J. Frost, S. A. McKeen, and F. C. Fehsenfeld (2007), A chemical ionization mass spectrometry technique for airborne measurements of ammonia, *J. Geophys. Res.*, 112, doi:10.1029/2006JD007589.

Pandis, S. N., R. A. Harley, G. R. Cass, and J. H. Seinfeld (1992), Secondary organic aerosol formation and transport, *Atmos. Environ.*, 26A, 2269-2282.

Pierce, J. R., K. Chen, and P. J. Adams (2007), Contribution of primary carbonaceous aerosol to cloud condensation nuclei: processes and uncertainties evaluated with a global aerosol microphysics model, *Atmos. Chem. Phys.*, 7, 5447-5466.

Saxena, P., and L. M. Hildemann (1996), Water-soluble organics in atmospheric particles: A critical review of the literature and application of thermodynamics to identify candidate compounds, *J. Atmos. Chem.*, 24, 57-109.

Smith, J. N., M. J. Dunn, T. M. VanReken, K. Iida, M. R. Stolzenburg, P. H. McMurry, and L. G. Huey (2008), Chemical composition of atmospheric nanoparticles formed from nucleation in Tecamac, Mexico: Evidence for an important role for organic species in nanoparticle growth, *Geophys. Res. Lett.*, 35, L04808, doi:10.1029/2007GL032523.

Sotiropoulou, R. E. P., E. Tagaris, C. Pilinis, T. Anttila, and M. Kulmala (2006), Modeling new particle formation during air pollution episodes: impacts on aerosol and cloud condensation nuclei, *Aerosol Sci. Tech.*, 40, 557-572.

Spracklen, D. V., K. S. Carslaw, M. Kulmala, V.-M. Kerminen, G. W. Mann, and S.-L. Sihto (2006), The contribution of boundary layer nucleation events to total particle concentrations on regional and global scales, *Atmos. Chem. Phys.*, 6, 5361-5648.

Spracklen, D. V., K. S. Carslaw, M. Kulmala, V.-M. Kerminen, S.-L. Sihto, I. Piipinen, J. Merikanto, G. W. Mann, M. P. Chipperfield, A. Wiedensohler, W. Birmili, and H. Lihavainen (2008), Contribution of particle formation to global cloud condensation nuclei concentrations, *Geophys. Res. Lett.*, 35, L06808, doi:10.1029/2007GL033038.

Stanier, C. O., A. Y. Khlystov, and S. N. Pandis (2004), Nucleation events during the Pittsburgh air quality study: Description and relation to key meteorological, gas-phase, and aerosol parameters, *Aerosol Sci. Tech.*, 38(S1), 253-264.

Stolzenburg, M. R., P. H. McMurry, H. Sakurai, J. N. Smith, R. L. Mauldin III, F. L. Eisele, and C. F. Clement (2005), Growth rates of freshly nucleated atmospheric particles in Atlanta, *J. Geophys. Res.* 110, D22S05, doi:10.1029/2005/JD005935.

Textor, C., M. Schulz, S. Guibert, S. Kinne, Y. Balkanski, S. Bauer, T. Berntsen, T. Berglen, O. Boucher, M. Chin, F. Dentener, T. Diehl, R. Easter, H. Feichter, D. Fillmore, S. Ghan, P. Ginoux, S. Gong, A. Grini, J. Hendricks, L. Horowitz, P. Huang, I. Isaksen, T. Iversen, S. Kloster, D. Koch, A. Kirkevåg, J. E. Kristiansson, M. Krol, A. Lauer, J. F. Lamarque, X. Liu, V. Montanaro, G. Myhre, J. Penner, G. Pitari, S. Reddy, Ø. Seland, P. Stier, T. Takemura, and X. Tie. (2006), Analysis and quantification of the diversities of aerosol life cycles within AeroCom, *Atmos. Chem. Phys.*, 6, 1777-1813.

Turco, R. P., J.-X. Zhao, and F. Yu (1998), A new source of tropospheric aerosols: Ion-ion recombination, *Geophys. Res. Lett.*, 25(5), 635-638.

Vehkamäki, H., M. Kulmala, I. Napari, K. E. J. Lehtinen, C. Timmreck, M. Noppel, and A. Laaksonen (2002), An improved parameterization for sulfuric acid-water nucleation rates for tropospheric and stratospheric conditions, *J. Geophys. Res.*, 107(D22), 4622, doi:10.1029/2002JD002184.

Weber, R. J., J. J. Marti, P. H. McMurry, F. L. Eisele, D. J. Tanner, and A. Jefferson (1996), Measured atmospheric new particle formation rates: Implications for nucleation mechanisms, *Chem. Engr. Comm.*, 151, 53-64.

Woo, K. S., D. R. Chen, D. Y. H. Pui, and P. H. McMurry (2001), Measurements of Atlanta aerosol size distributions: Observations of ultrafine particle events, *Aerosol Sci. Tech.*, 34, 75-87.

Yu, F. (2002), Altitude variations of cosmic ray induced production of aerosols: Implications for global cloudiness and climate, *J. Geophys. Res.*, 107(A7), 1118, doi:10.1029/2001JA000248.

Yu, F., Z. Wang, G. Luo, and R. Turco (2008), Ion-mediated nucleation as an important source of tropospheric aerosols, *Atmos. Chem. Phys.*, 8, 2537-2554.

Zhang, K. M., and A. S. Wexler (2002), Modeling the number distributions of urban and regional aerosols: theoretical foundations, *Atmos. Environ.*, 36, 1863-1874.

Zhang, K. M., and A. S. Wexler (2004), Evolution of particle number distributions near roadways—Part I: Analysis of aerosol dynamics and its implication for engine emissions measurement, *Atmos. Environ.*, 38, 6643-6653.

Zhang, K. M., A. S. Wexler, Y. F. Zhu, W. C. Hinds, and C. Sioutas (2004), Evolution of particle number distributions near roadways. Part II: the "Road-to-Ambient" process, *Atmos. Environ.*, 38, 6655-6665.

Zhang, Q., J. L. Jimenez, M. R. Canagaratna, J. D. Allan, H. Coe, I. Ulbrich, M, RAlfarra, A. Takami, A. M. Middlebrook, Y. L. Sun, K. Dzepina, E. Dunlea, K. Docherty, P. F. DeCarlo, D. Salcedo, T. Onasch, J. T. Jayne, T. Miyoshi, A. Shimono, S. Hatakeyama, N. Takegawa, Y. Kondo, J. Schneider, F. Drewnick, S. Borrmann, S. Weimer, K. Demerjian, P. Williams, K. Bower, R. Bahreini, L. Cottrell, R. J. Griffin, J. Rautiainen, J. Y. Sun, Y. M. Zhang, and D. R. Worsnop (2007), Ubiquity and dominance of oxygenated species in organic aerosols in anthropogenically-influenced Northern Hemisphere midlatitudes, *Geophys. Res. Lett.*, 34, L13801, doi:10.1029/2007GL029979.

Figures

Figure 1. New particle formation rate J_{NPF} versus sulfuric acid concentration [H_2SO_4] for the several new particle formation parameterizations considered here at 25ºC and relative humidity 50%: a) without background aerosols; b) with high concentration of background aerosols: a lognormal with $N_{\mathrm{tot}} = 500\ \mathrm{cm}^{-3}$, $\sigma_{\mathrm{g}} = 1.5$, and $D_{\mathrm{g}} = 150$ nm, corresponding to a rate constant for condensational sink for sulfuric acid of $k_{\mathrm{cs}} = 2\cdot10^{-2}\ \mathrm{s}^{-1}$. The effect of background aerosols on J_{NPF} was not considered for EM97.

Figure 2. Probability distribution function of J_{NPF}, $dF/d\log J_{\mathrm{NPF}}$, the fraction of occurrences over the entire modeling domain and period that are within a given logarithmic range of J_{NPF}, as a function of new particle formation rate J_{NPF}: a) calculated with THN+NIIR using the standard CMAQ operator-splitting algorithm; b) calculated with THN+NIIR using the steady-state H_2SO_4 concentration obtained for new particle formation and condensation occurring simultaneously; c) calculated for THN+NIIR without the steady-state assumption for H_2SO_4, d) calculated for NIIR acting alone without the steady-state assumption for H_2SO_4. Red denotes calculations with "mass cap" that limits J_{NPF} to the amount of H_2SO_4 formed in the time interval; gray denotes calculations without the mass cap.

Figure 3. Spatial distribution of primary emission fluxes for NPF precursors, SO_2 and NH_3, for 1 July, 2004.

Figure 4. Model domain with simulated wind field, averaged over July, 2004, at an elevation corresponding to 85% of the surface pressure. Red circles denote sensitivity analysis sites, A: northwestern Iowa (96.2ºW, 43.5ºN); B: near New Haven, Connecticut (72.9ºW, 41.1ºN); C: near Acadia National Park, Maine (68.1ºW, 43.7ºN); D: 350 km southeast of Cape Cod, Massachusetts (66.5ºW, 39.9ºN).

Figure 5(a). Time series of T, RH, [SO_2], [NH_3], [H_2SO_4], J_{NPF}, F_{KK}, N_{ATK}, V_{ATK}, N_{ACC}, $D_{\mathrm{g,ATK}}$, $D_{\mathrm{g,ACC}}$, rate of IMT of aerosol number, intramodal coagulation rates for the Aitken and the accumulation modes, dry-air molar mixing ratios of sulfate and ammonium in the Aitken and accumulation modes, mass concentration of secondary organic aerosol SOA in the Aitken mode, wet deposition flux of accumulation mode particle number, and dry deposition flux of Aitken mode particle number at the lowest level (0-20 m above the ground) for different model variants at Site A during July, 2004. Tick marks denote midnight UTC; dashed vertical blue lines denote local noon. THN (black) is plotted last and may obscure traces of other model variants. The quantities $D_{g,ATK}$, $D_{g,ACC}$, and V_{ATK} are reported for dry particles, although for use in evaluation of coagulation rates, etc., they were calculated for particles at their ambient (i.e., wet) sizes. Abundances of [SO_2], [NH_3], [SO_4^{2-}], and [NH_4^+] are presented as molar mixing ratios in dry air, nmol mol^{-1} (ppb, parts per billion). At 298 K and 1 atm, a molar mixing ratio of 1 ppb is equivalent to a mass concentration of 3.9 μg m^{-3} for sulfate, and to 0.74 μg m^{-3} for ammonium.

Figure 5(b). Same as Fig. 5(a) except for Site B, with SO_2 mixing ratio measurements from EPA monitoring stations at Meriden and Waterbury, Connecticut. Note the different scale for some quantities such as [SO_2].

Figure 5(c). Same as Fig. 5(a) except for Site C, with SO_2 mixing ratio measurements from EPA monitoring stations at Oxford and Portland, Maine.

Figure 5(d). Same as Fig. 5(a) except for Site D.

Figure 6. Vertical profiles of [H_2SO_4], [NH_3], T and RH, J_{NPF}, N_{ATK}, and $D_{g,ATK}$ at local noon for different model variants, averaged over July, 2004 at Site B. Abundance of [NH_3] is presented as molar mixing ratio in dry air, pmol mol^{-1} (ppt, parts per trillion).

Figure 7. IMT fraction, the fraction of time intervals for which IMT occurred anywhere in the columns over the four sites shown in Fig. 4 during July, 2004, in percent, as a function of (a) J_{NPF}, and (b) [H_2SO_4] for J_{NPF} in the range 10-100 cm^{-3} s^{-1}.

Figure 8. Spatial distribution of daily-average J_{NPF} and N_{ATK} in the planetary boundary layer (PBL) and in the free troposphere (FT) for the different model variants on 20 July, 2004.

Figure 9. Time series of [H_2SO_4], J_{NPF}, F_{KK}, N_{ATK}, A_{ATK}, V_{ATK}, N_{ACC}, $D_{g,ATK}$, $D_{g,ACC}$, rate of IMT of aerosol number, intramodal coagulation rates for the Aitken and the accumulation modes, dry-air molar mixing ratios of sulfate and ammonium in the Aitken and accumulation modes, mass concentrations of secondary organic aerosol (SOA) in the Aitken and the accumulation modes, wet deposition flux of accumulation mode particle number, and dry deposition flux of Aitken mode particle number at the lowest level (0-20 m above the ground) for THN+NIIR at Site B during July, 2004, with mass emissions at $D_{g,ATK} = 30$ nm and $D_{g,ACC} = 300$ nm (D_0 case), and

for $D\times2$ and $D/2$ cases. The quantities $D_{\mathrm{g,ATK}}$, $D_{\mathrm{g,ACC}}$, A_{ATK}, and V_{ATK} are reported for dry particles, although for use in evaluation of coagulation rates, etc., they were calculated for particles at their ambient (i.e., wet) sizes. Abundances of $[\mathrm{SO_4}^{2-}]$ and $[\mathrm{NH_4}^{+}]$ are presented as dry-air molar mixing ratios in nmol mol^{-1} (ppb, parts per billion); at 298 K and 1 atm, a molar mixing ratio of 1 ppb is equivalent to a mass concentration of 3.9 µg m^{-3} for sulfate, and to 0.74 µg m^{-3} for ammonium. Lines denoting factor of 8 in N_{ACC}, and N_{ATK}, factor of 2 in $D_{\mathrm{g,ACC}}$, $D_{\mathrm{g,ATK}}$, and A_{ATK}, and factor of 128 in intramodal coagulation rates $\mathrm{Coag}_{\mathrm{ATK\text{-}ATK}}$ and $\mathrm{Coag}_{\mathrm{ACC\text{-}ACC}}$ are shown. Green circle represents instance of $D_{\mathrm{g,ATK}}$ being largest in the $D\times2$ case; brown circle represents instance of $D_{\mathrm{g,ATK}}$ being largest in the $D/2$ case.

Figure 10. Production and loss rates of aerosol particle number concentration in the Aitken and accumulation modes by different processes for the different model variants averaged over the entire modeling domain and time period.

Figure 11. Flight paths of the NOAA WP-3D aircraft during the ICARTT 2004 study. Inner box denotes the domain of the 12 km resolution model.

Figure 12. Comparison of measurements taken from aircraft (gray shaded regions) of concentrations of number N, surface area A, and volume V with results of different model variants for eight selected days during the ICARTT 2004 study. Measured concentrations are for (dry) diameters from 3 nm to 2.5 µm; modeled values are calculated using ambient (wet) diameters, but reported for dry diameters, as the sum of the concentrations in the Aitken and accumulation modes. Height refers to height above mean sea level. Orange bands are used to denote some period of poor performance, and brown circles to denote some periods of good performance.

Figure 13. Comparison between measurements taken from aircraft and model simulations for both the 60 km resolution and the 12 km resolution for THN+NIIR on 20 July, 2004. Concentrations of gaseous species are given as dry-air molal mixing ratios in nmol mol^{-1} (ppb, parts per billion), except for $[\mathrm{NH_3}]$, which is in pmol mol^{-1} (ppt, parts per trillion). Measured concentrations of particle number N, surface area A, and volume V are for (dry) diameters from 3 nm to 2.5 µm; modeled values are calculated using ambient (wet) diameters, but reported for dry diameters, as the sum of the concentrations in the Aitken and accumulation modes. Height

refers to height above mean sea level. The last three panels compare the size distribution of aerosol number concentration for diameter from 2 nm to 1 μm.

Table 1. Model variants and their descriptions

Model variant	Nucleation formulation	$\frac{D_{\mathrm{g,emission}}}{D_{\mathrm{g,emission,BASE}}}$
BASE	None	1
BHNV	BHN (Vehkamäki et al.)	1
BHNJ	BHN (Jaecker-Voirol & Mirabel)	1
NIIR	NIIR (Turco et al.)	1
EM97	Empirical NPF parameterization (Eisele & McMurry)	1
THN	THN (Napari et al.)	1
D_0	THN + NIIR	1
$D/2$	THN + NIIR	0.5
$D\times2$	THN + NIIR	2

Table 2. Time- and domain- averaged number concentrations in the Aitken and accumulation modes and their turnover times for all model variants.

Model variant	Aitken mode		Accumulation mode	
	$N_{\mathrm{ATK}}/\mathrm{cm}^{-3}$	$\tau_{\mathrm{N,ATK}}/\mathrm{d}$	$N_{\mathrm{ACC}}/\mathrm{cm}^{-3}$	$\tau_{\mathrm{N,ACC}}/\mathrm{d}$
BASE	3	2.8	33	2.7
BHNV	20	0.51	34	2.7
BHNJ	139	0.54	39	2.7
NIIR	99	0.20	36	2.7
EM97	517	0.15	48	2.6
THN	2581	0.035	60	2.8
D_0	2436	0.033	60	2.7
$D/2$	1863	0.031	169	1.6
$D\times2$	3251	0.037	35	3.1

Fig. 1

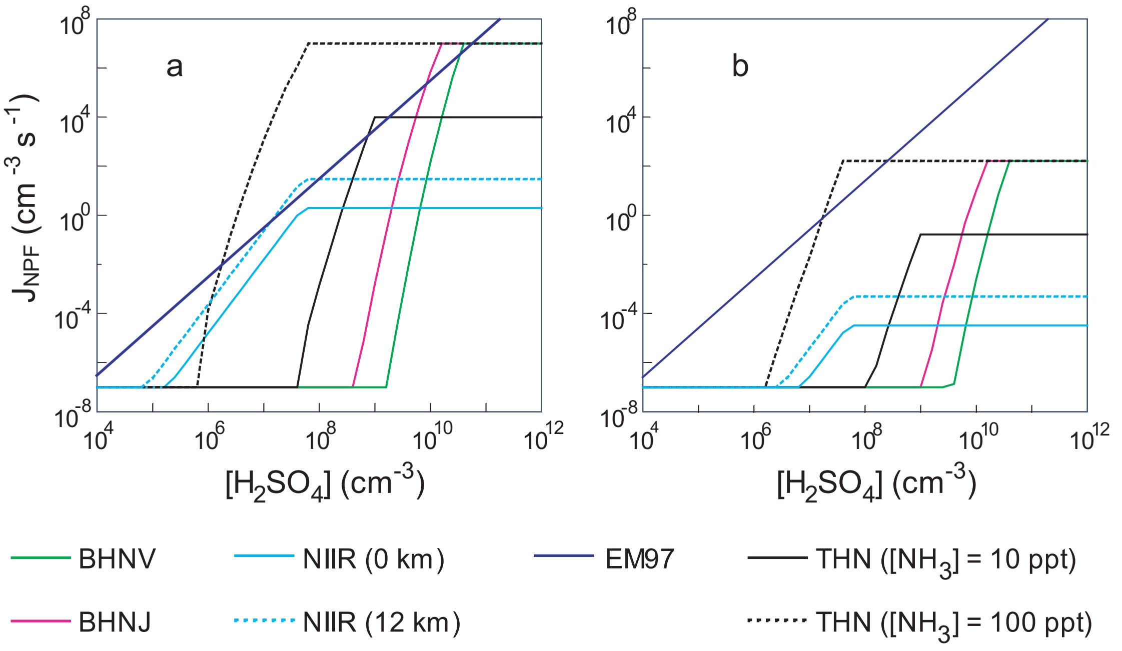

a
b
J_{NPF} (cm^{-3} s^{-1})
10^{8}
10^{4}
10^{0}
10^{-4}
10^{-8}
10^{4}
10^{6}
10^{8}
10^{10}
10^{12}
[H_2SO_4] (cm^{-3})
BHNV
BHNJ
NIIR (0 km)
NIIR (12 km)
EM97
THN ([NH_3] = 10 ppt)
THN ([NH_3] = 100 ppt)

Fig. 2

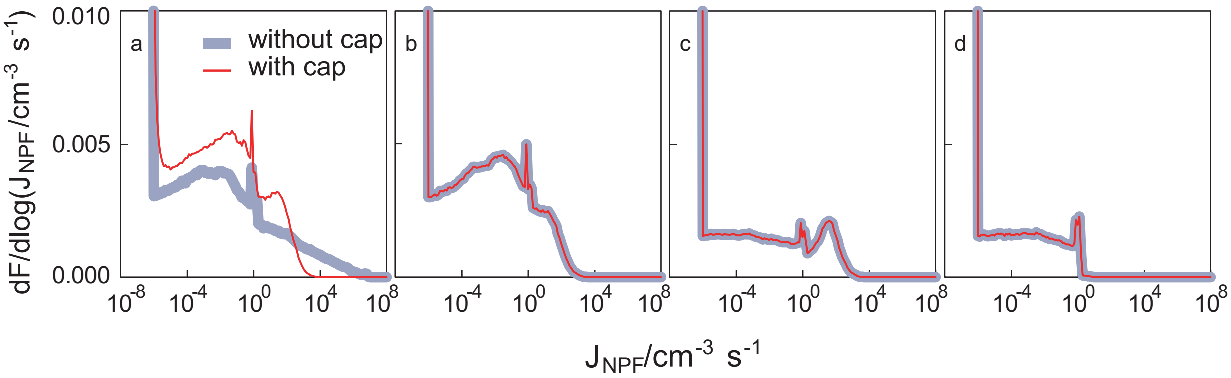
dF/dlog(J_{NPF}/cm^{-3} s^{-1})
0.010
0.005
0.000
a
b
c
d
without cap
with cap
10^{-8}
10^{-4}
10^{0}
10^{4}
10^{8}
J_{NPF}/cm^{-3} s^{-1}

Fig. 3

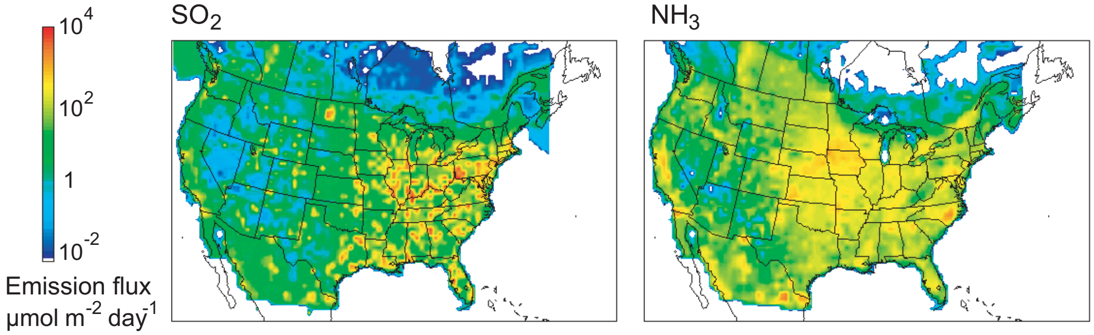
SO$_2$
NH$_3$
10^4
10^2
1
10^{-2}
Emission flux
μmol m^{-2} day^{-1}

Fig. 4

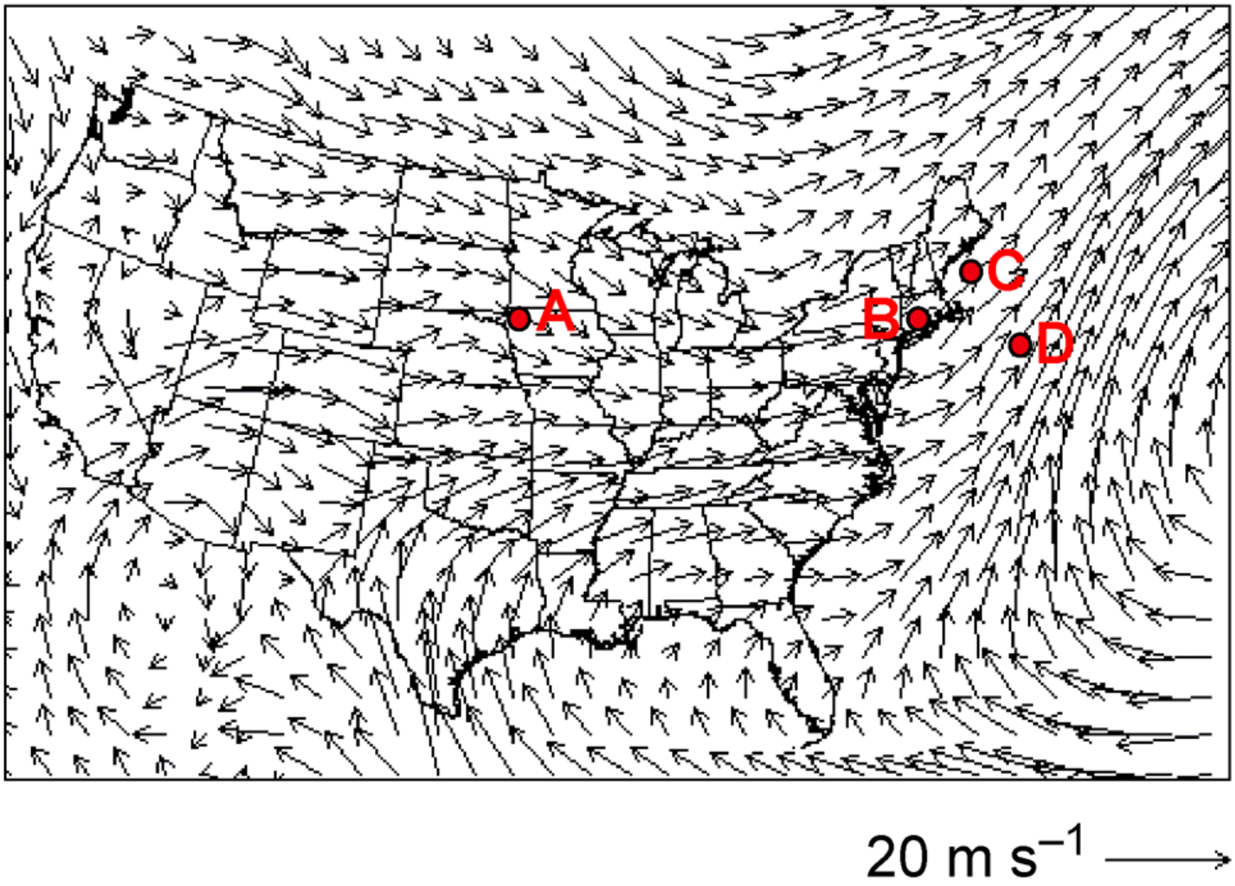

Fig. 5a

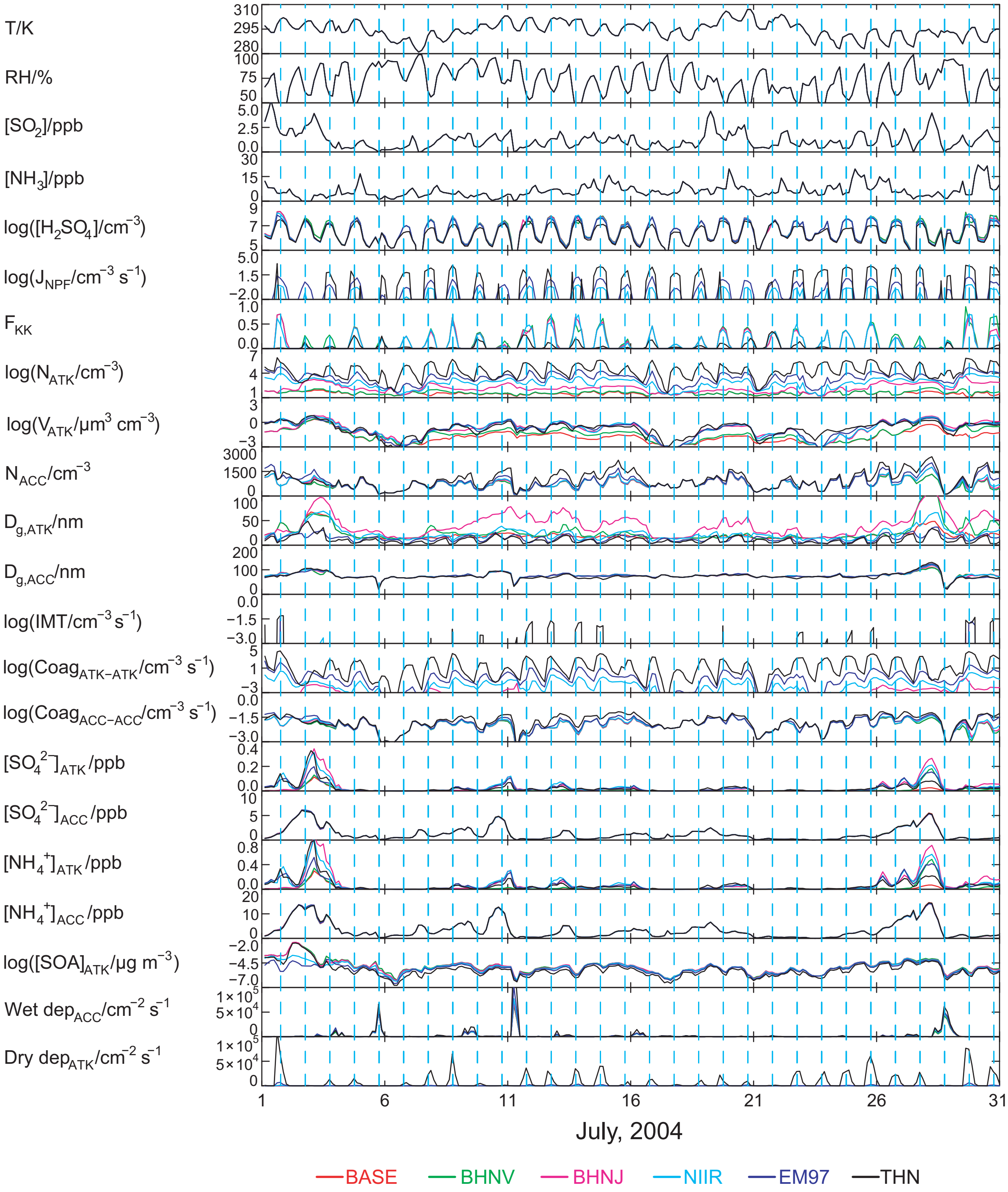
T/K
310
295
280
RH/%
100
75
50
[SO$_2$]/ppb
5.0
2.5
0.0
[NH$_3$]/ppb
30
15
0
log([H$_2$SO$_4$]/cm^{-3})
9
7
5
log(J$_{NPF}$/cm^{-3} s^{-1})
5.0
1.5
−2.0
F$_{KK}$
1.0
0.5
0.0
log(N$_{ATK}$/cm^{-3})
7
4
1
log(V$_{ATK}$/μm^3 cm^{-3})
3
0
−3
N$_{ACC}$/cm^{-3}
3000
1500
0
D$_{g,ATK}$/nm
100
50
0
D$_{g,ACC}$/nm
200
100
0
log(IMT/cm^{-3} s^{-1})
0.0
−1.5
−3.0
log(Coag$_{ATK-ATK}$/cm^{-3} s^{-1})
5
1
−3
log(Coag$_{ACC-ACC}$/cm^{-3} s^{-1})
0.0
−1.5
−3.0
[SO$_4^{2-}$]$_{ATK}$/ppb
0.4
0.2
0.0
[SO$_4^{2-}$]$_{ACC}$/ppb
10
5
0
[NH$_4^+$]$_{ATK}$/ppb
0.8
0.4
0.0
[NH$_4^+$]$_{ACC}$/ppb
20
10
0
log([SOA]$_{ATK}$/μg m^{-3})
−2.0
−4.5
−7.0
Wet dep$_{ACC}$/cm^{-2} s^{-1}
1×10^5
5×10^4
0
Dry dep$_{ATK}$/cm^{-2} s^{-1}
1×10^5
5×10^4
0
1
6
11
16
21
26
31
July, 2004
BASE
BHNV
BHNJ
NIIR
EM97
THN

Fig. 5b

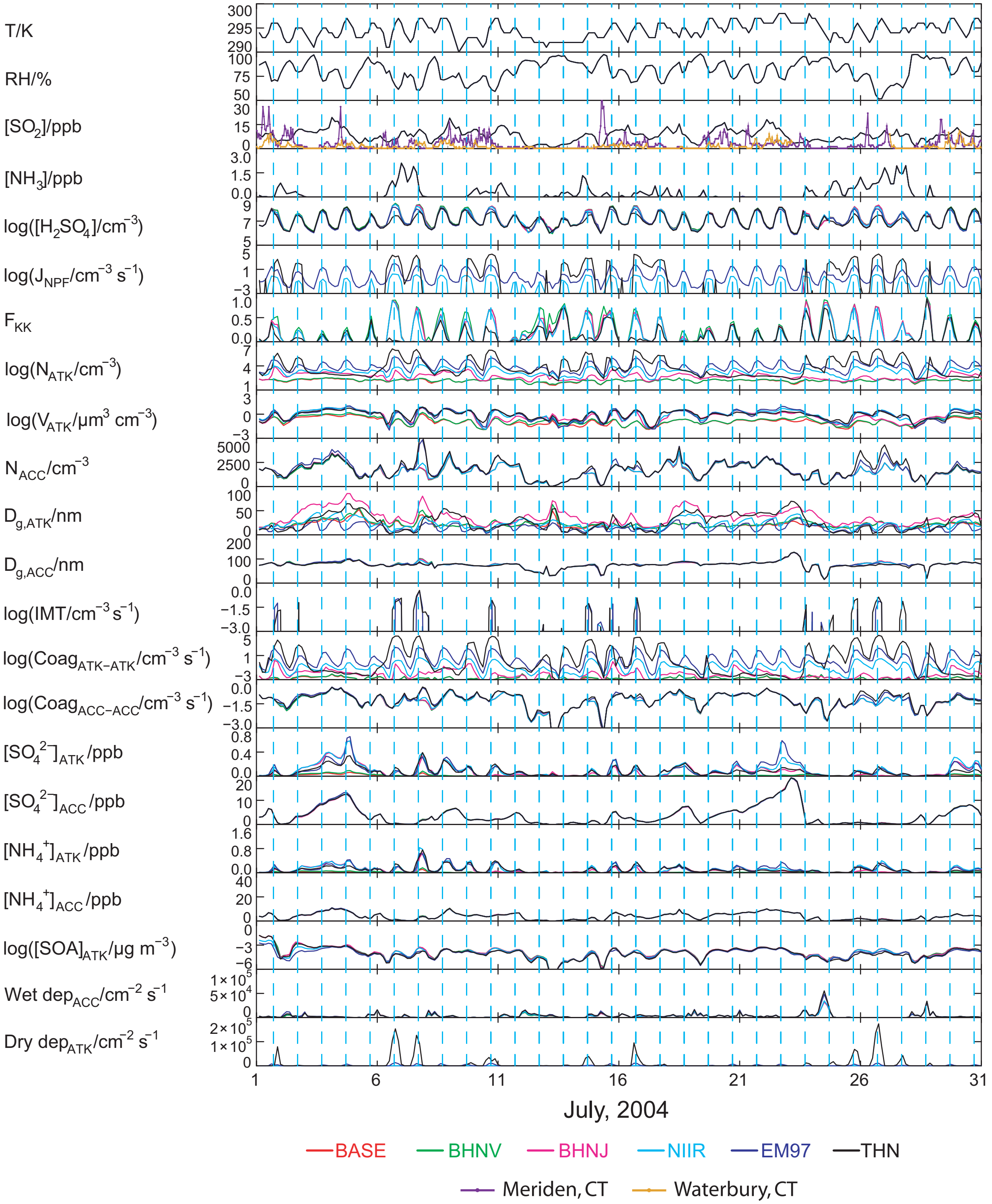

T/K
300
295
290
RH/%
100
75
50
[SO2]/ppb
30
15
0
[NH3]/ppb
3.0
1.5
0.0
log([H2SO4]/cm−3)
9
7
5
log(JNPF/cm−3 s−1)
5
1
−3
FKK
1.0
0.5
0.0
log(NATK/cm−3)
7
4
1
log(VATK/μm3 cm−3)
3
0
−3
NACC/cm−3
5000
2500
0
Dg,ATK/nm
100
50
0
Dg,ACC/nm
200
100
0
log(IMT/cm−3 s−1)
0.0
−1.5
−3.0
log(CoagATK−ATK/cm−3 s−1)
5
1
−3
log(CoagACC−ACC/cm−3 s−1)
0.0
−1.5
−3.0
[SO42−]ATK/ppb
0.8
0.4
0.0
[SO42−]ACC/ppb
20
10
0
[NH4+]ATK/ppb
1.6
0.8
0.0
[NH4+]ACC/ppb
40
20
0
log([SOA]ATK/μg m−3)
0
−3
−6
Wet depACC/cm−2 s−1
1×105
5×104
0
Dry depATK/cm−2 s−1
2×105
1×105
0
1
6
11
16
21
26
31
July, 2004
BASE
BHNV
BHNJ
NIIR
EM97
THN
Meriden, CT
Waterbury, CT

Fig. 5c

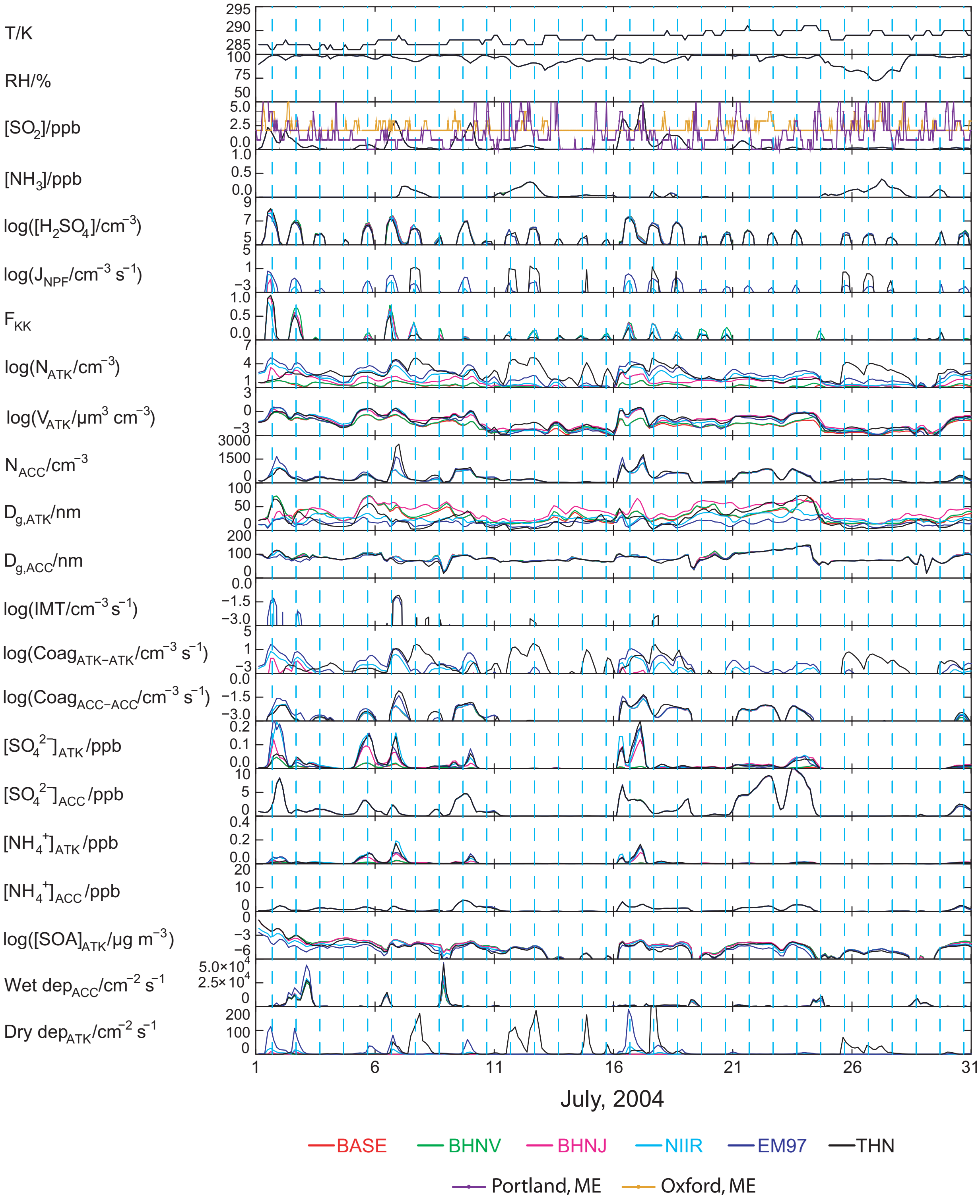
T/K
295
290
285
RH/%
100
75
50
$[SO_2]$/ppb
5.0
2.5
0.0
$[NH_3]$/ppb
1.0
0.5
0.0
$\log([H_2SO_4]/cm^{-3})$
9
7
5
$\log(J_{NPF}/cm^{-3}\ s^{-1})$
5
1
−3
F_{KK}
1.0
0.5
0.0
$\log(N_{ATK}/cm^{-3})$
7
4
1
$\log(V_{ATK}/\mu m^3\ cm^{-3})$
3
0
−3
N_{ACC}/cm^{-3}
3000
1500
0
$D_{g,ATK}$/nm
100
50
0
$D_{g,ACC}$/nm
200
100
0
$\log(IMT/cm^{-3}\ s^{-1})$
0.0
−1.5
−3.0
$\log(Coag_{ATK-ATK}/cm^{-3}\ s^{-1})$
5
1
−3
$\log(Coag_{ACC-ACC}/cm^{-3}\ s^{-1})$
0.0
−1.5
−3.0
$[SO_4^{2-}]_{ATK}$/ppb
0.2
0.1
0.0
$[SO_4^{2-}]_{ACC}$/ppb
10
5
0
$[NH_4^+]_{ATK}$/ppb
0.4
0.2
0.0
$[NH_4^+]_{ACC}$/ppb
20
10
0
$\log([SOA]_{ATK}/\mu g\ m^{-3})$
0
−3
−6
Wet $dep_{ACC}/cm^{-2}\ s^{-1}$
5.0×10^4
2.5×10^4
0
Dry $dep_{ATK}/cm^{-2}\ s^{-1}$
200
100
0
1
6
11
16
21
26
31
July, 2004
BASE
BHNV
BHNJ
NIIR
EM97
THN
Portland, ME
Oxford, ME

Fig. 5d

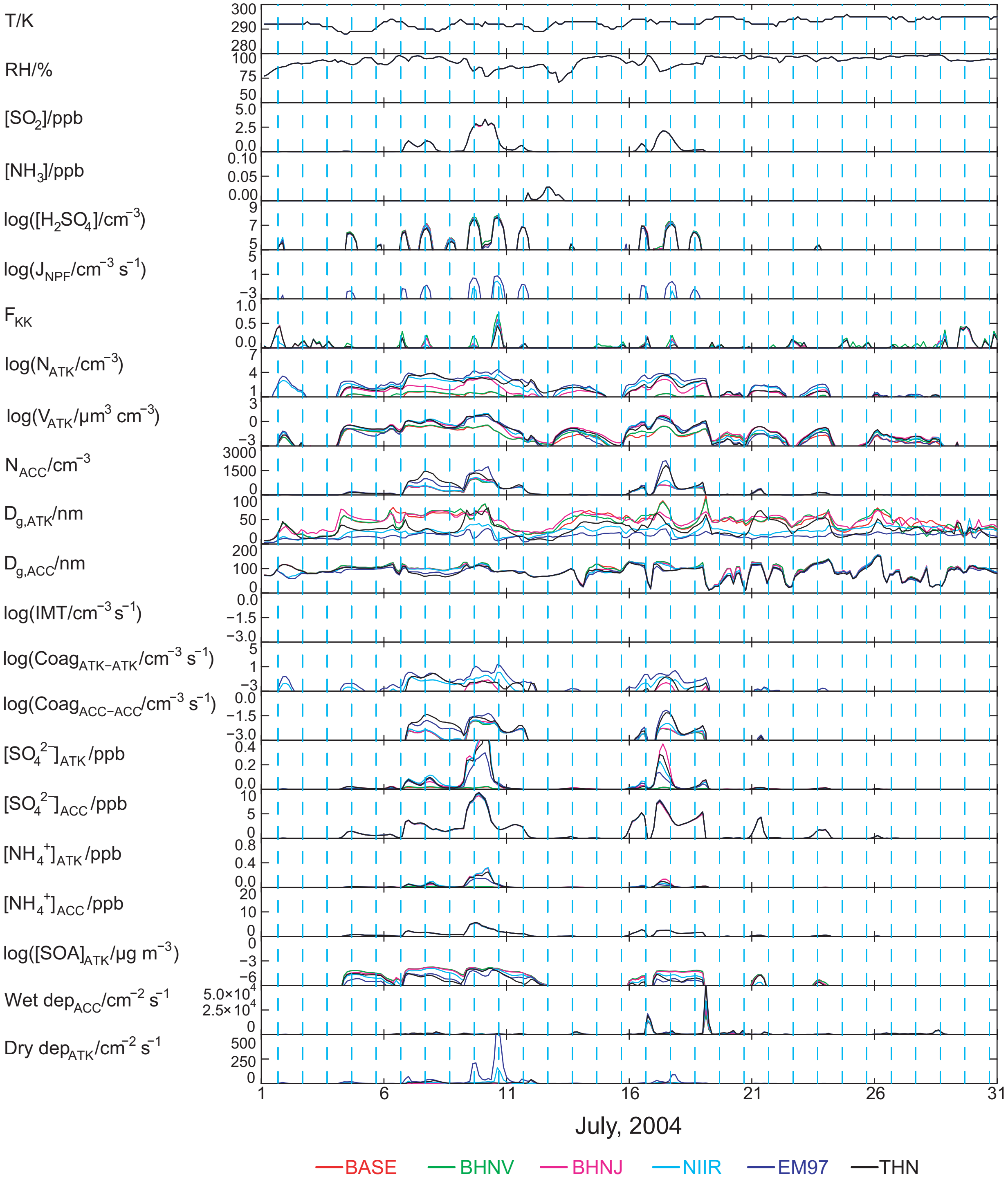
T/K
300
290
280
RH/%
100
75
50
[SO$_2$]/ppb
5.0
2.5
0.0
[NH$_3$]/ppb
0.10
0.05
0.00
log([H$_2$SO$_4$]/cm^{-3})
9
7
5
log(J$_{NPF}$/cm^{-3} s^{-1})
5
1
−3
F$_{KK}$
1.0
0.5
0.0
log(N$_{ATK}$/cm^{-3})
7
4
1
log(V$_{ATK}$/μm^3 cm^{-3})
3
0
−3
N$_{ACC}$/cm^{-3}
3000
1500
0
D$_{g,ATK}$/nm
100
50
0
D$_{g,ACC}$/nm
200
100
0
log(IMT/cm^{-3} s^{-1})
0.0
−1.5
−3.0
log(Coag$_{ATK-ATK}$/cm^{-3} s^{-1})
5
1
−3
log(Coag$_{ACC-ACC}$/cm^{-3} s^{-1})
0.0
−1.5
−3.0
[SO$_4^{2-}$]$_{ATK}$/ppb
0.4
0.2
0.0
[SO$_4^{2-}$]$_{ACC}$/ppb
10
5
0
[NH$_4^+$]$_{ATK}$/ppb
0.8
0.4
0.0
[NH$_4^+$]$_{ACC}$/ppb
20
10
0
log([SOA]$_{ATK}$/μg m^{-3})
0
−3
−6
Wet dep$_{ACC}$/cm^{-2} s^{-1}
5.0×10^4
2.5×10^4
0
Dry dep$_{ATK}$/cm^{-2} s^{-1}
500
250
0
1
6
11
16
21
26
31
July, 2004
BASE
BHNV
BHNJ
NIIR
EM97
THN

Fig. 6

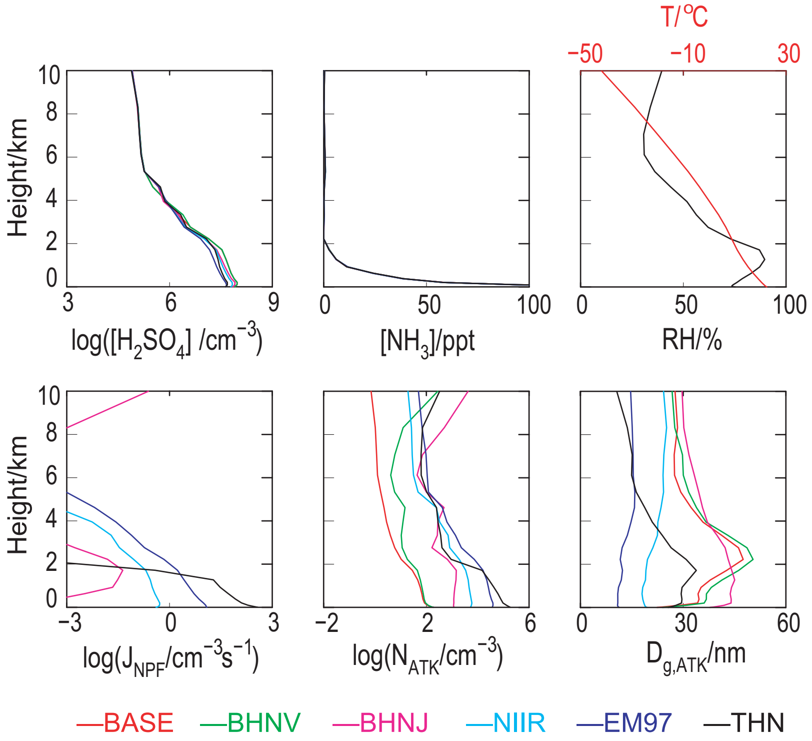

Height/km
10
8
6
4
2
0
3
6
9
$\log([H_2SO_4]\ /cm^{-3})$
0
50
100
$[NH_3]$/ppt
T/°C
−50
−10
30
0
50
100
RH/%
Height/km
10
8
6
4
2
0
−3
0
3
$\log(J_{NPF}/cm^{-3}s^{-1})$
−2
2
6
$\log(N_{ATK}/cm^{-3})$
0
30
60
$D_{g,ATK}$/nm
—BASE
—BHNV
—BHNJ
—NIIR
—EM97
—THN

Fig. 7

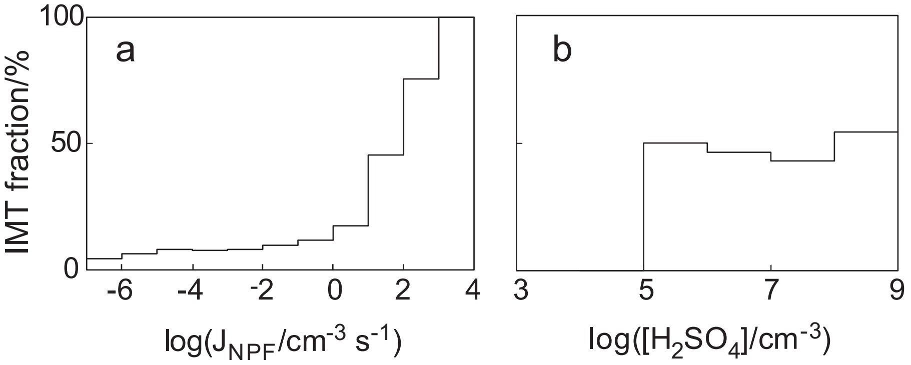
a
b
IMT fraction/%
100
50
0
-6
-4
-2
0
2
4
3
5
7
9
log(J_{NPF}/cm^{-3} s^{-1})
log([H_2SO_4]/cm^{-3})

Fig. 8

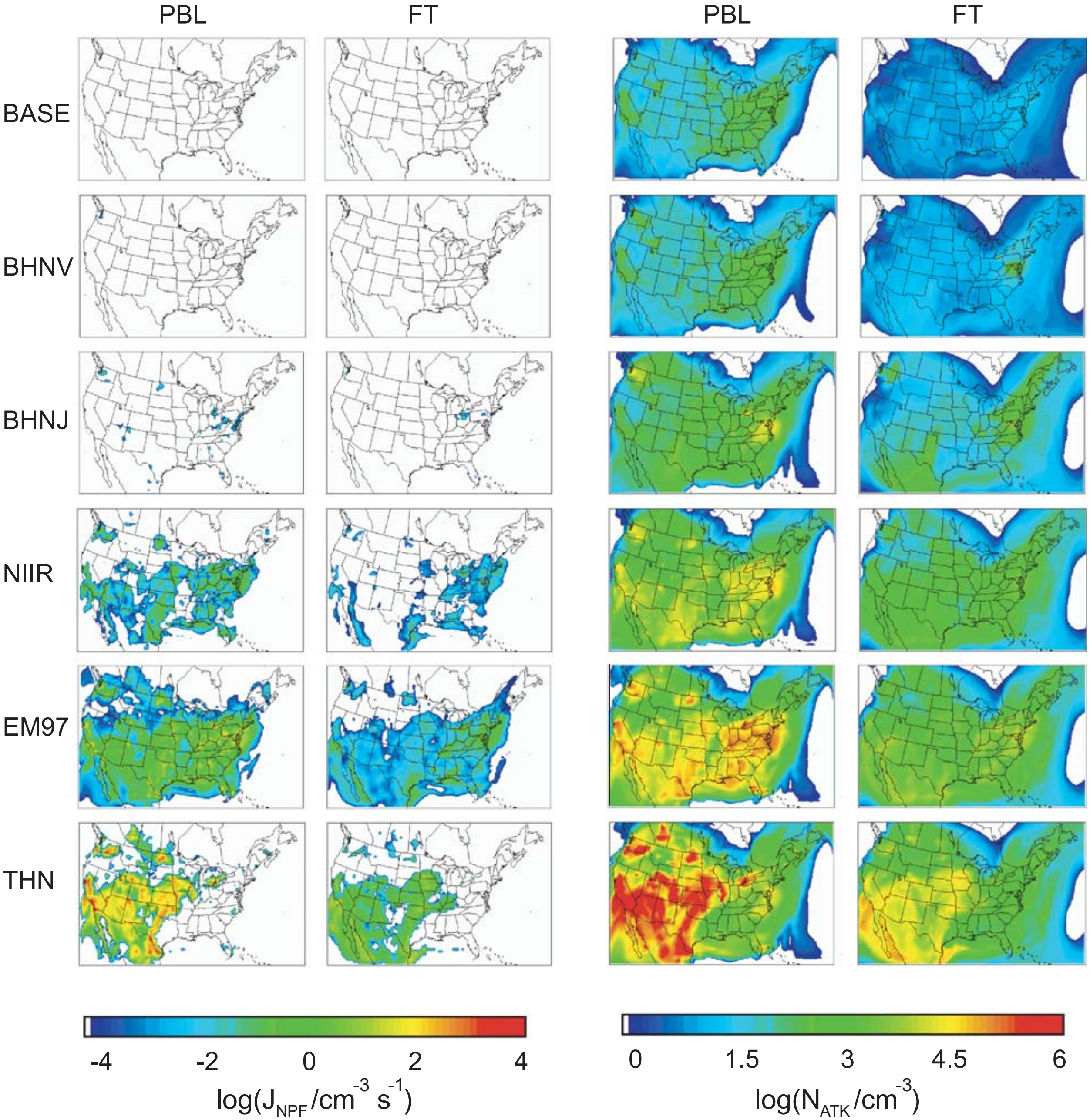
PBL
FT
PBL
FT
BASE
BHNV
BHNJ
NIIR
EM97
THN
-4
-2
0
2
4
log(J_{NPF}/cm^{-3} s^{-1})
0
1.5
3
4.5
6
log(N_{ATK}/cm^{-3})

Fig. 9

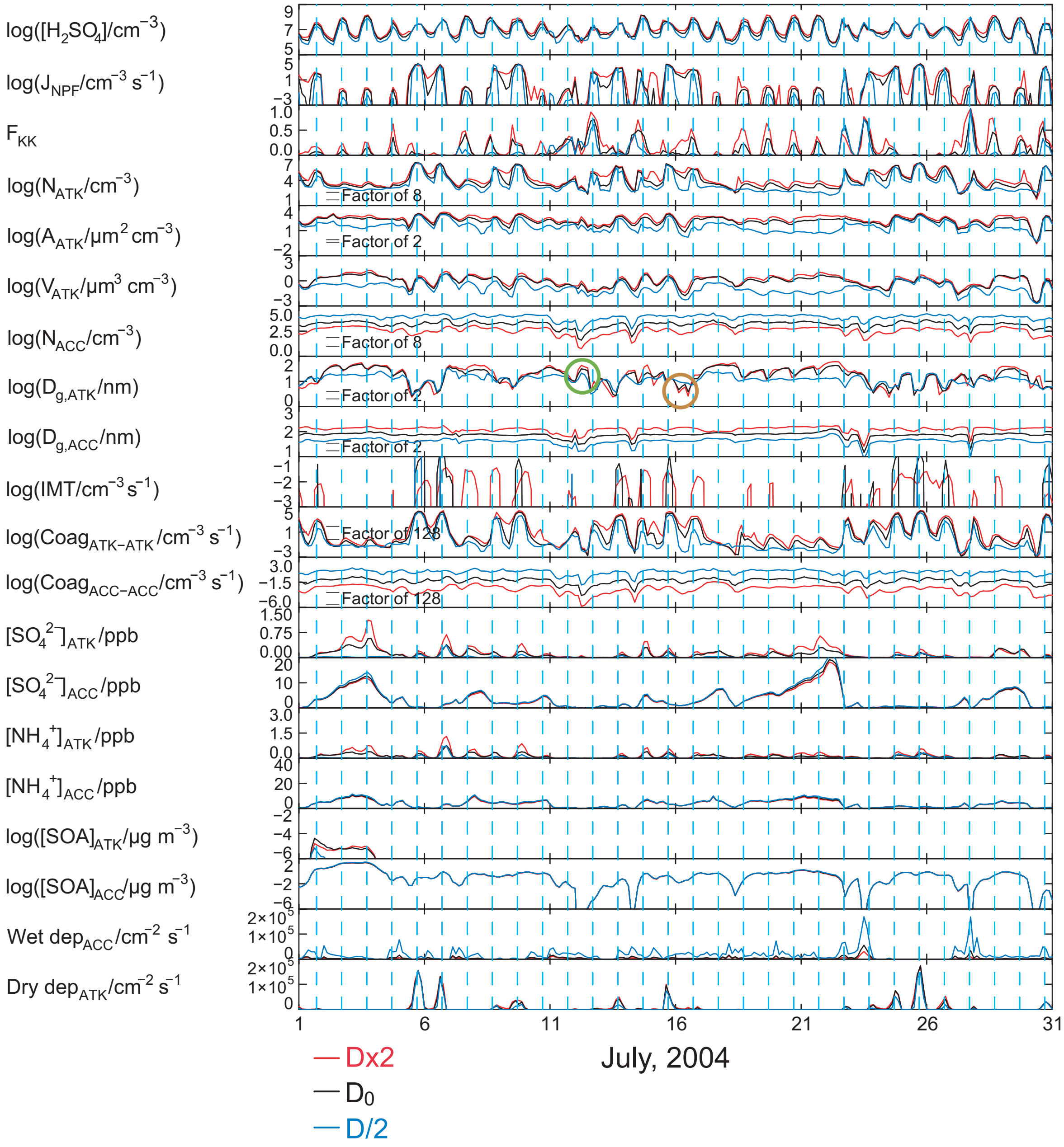

$\log([H_2SO_4]/cm^{-3})$
$\log(J_{NPF}/cm^{-3}\ s^{-1})$
F_{KK}
$\log(N_{ATK}/cm^{-3})$
$\log(A_{ATK}/\mu m^2\ cm^{-3})$
$\log(V_{ATK}/\mu m^3\ cm^{-3})$
$\log(N_{ACC}/cm^{-3})$
$\log(D_{g,ATK}/nm)$
$\log(D_{g,ACC}/nm)$
$\log(IMT/cm^{-3}\ s^{-1})$
$\log(Coag_{ATK-ATK}/cm^{-3}\ s^{-1})$
$\log(Coag_{ACC-ACC}/cm^{-3}\ s^{-1})$
$[SO_4^{2-}]_{ATK}/ppb$
$[SO_4^{2-}]_{ACC}/ppb$
$[NH_4^+]_{ATK}/ppb$
$[NH_4^+]_{ACC}/ppb$
$\log([SOA]_{ATK}/\mu g\ m^{-3})$
$\log([SOA]_{ACC}/\mu g\ m^{-3})$
$Wet\ dep_{ACC}/cm^{-2}\ s^{-1}$
$Dry\ dep_{ATK}/cm^{-2}\ s^{-1}$
9
7
5
5
1
−3
1.0
0.5
0.0
7
4
1
Factor of 8
4
1
−2
Factor of 2
3
0
−3
5.0
2.5
0.0
Factor of 8
2
1
0
Factor of 2
3
2
1
Factor of 2
−1
−2
−3
5
1
−3
Factor of 128
3.0
−1.5
−6.0
Factor of 128
1.50
0.75
0.00
20
10
0
3.0
1.5
0.0
40
20
0
−2
−4
−6
2
−2
−6
2×10^5
1×10^5
0
2×10^5
1×10^5
0
1
6
11
16
21
26
31
July, 2004
Dx2
D$_0$
D/2

Fig. 10

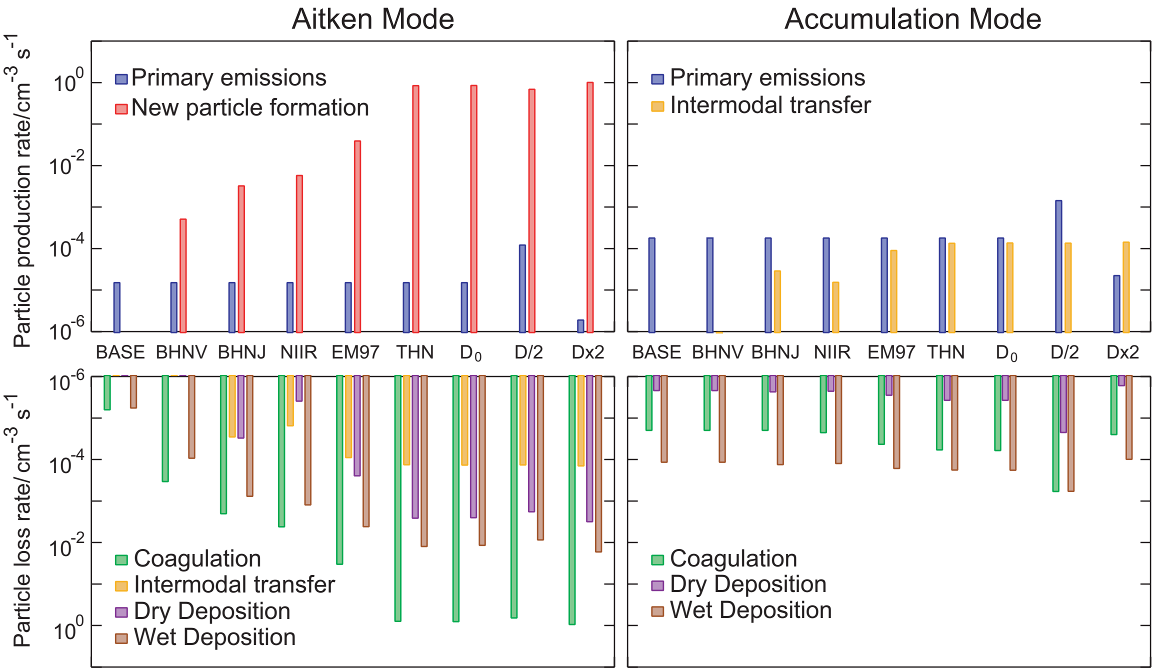

Aitken Mode
Accumulation Mode
Particle production rate/cm-3 s-1
Particle loss rate/cm-3 s-1
10^0
10^-2
10^-4
10^-6
Primary emissions
New particle formation
Intermodal transfer
BASE
BHNV
BHNJ
NIIR
EM97
THN
D0
D/2
Dx2
Coagulation
Dry Deposition
Wet Deposition

Fig. 11

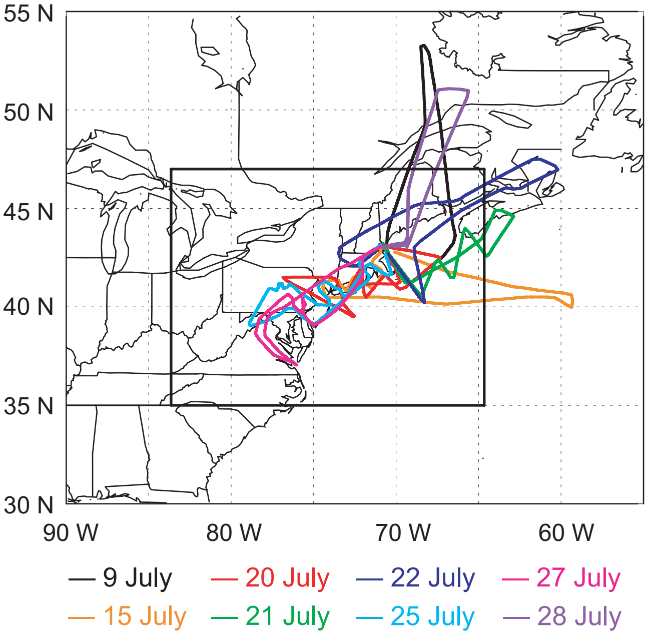

55 N
50 N
45 N
40 N
35 N
30 N
90 W
80 W
70 W
60 W
— 9 July
— 20 July
— 22 July
— 27 July
— 15 July
— 21 July
— 25 July
— 28 July

Fig. 12

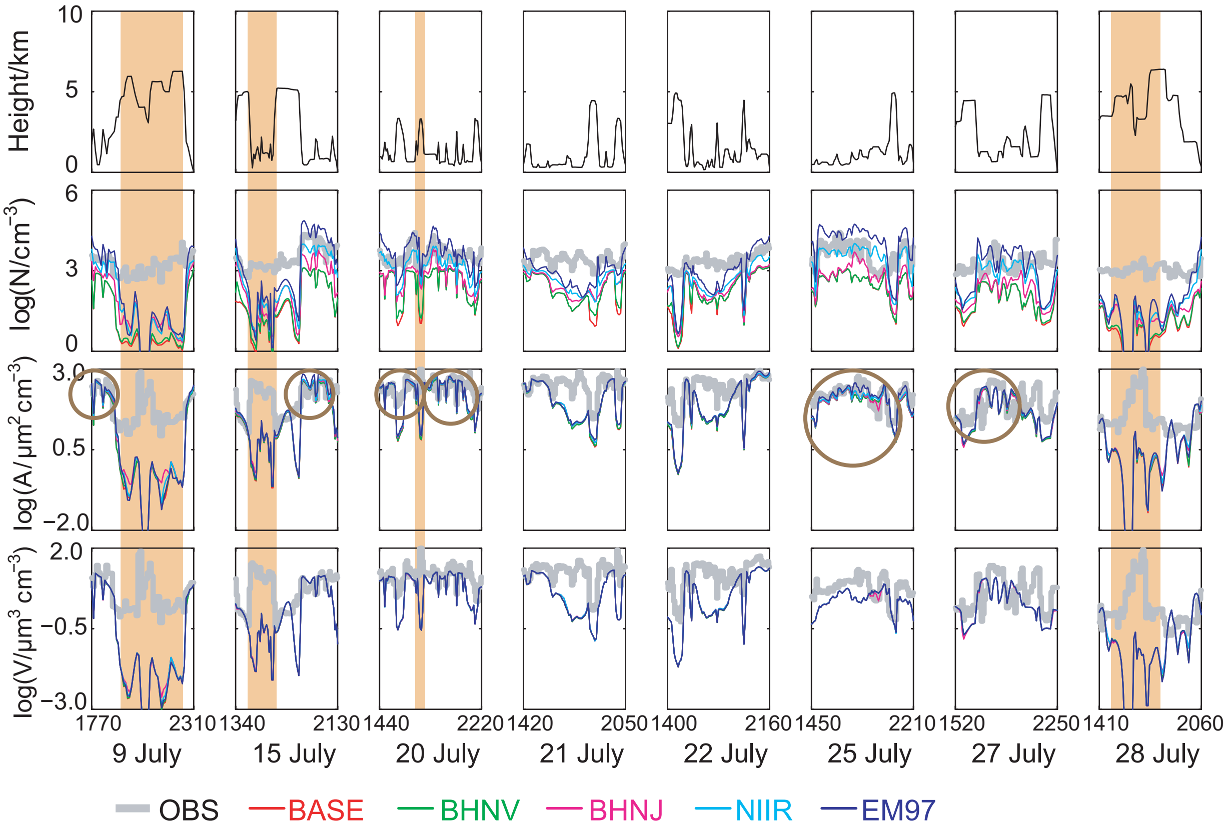
Height/km
10
5
0
log(N/cm^{-3})
6
3
0
log(A/μm^{2}cm^{-3})
3.0
0.5
−2.0
log(V/μm^3 cm^{-3})
2.0
−0.5
−3.0
1770
2310
1340
2130
1440
2220
1420
2050
1400
2160
1450
2210
1520
2250
1410
2060
9 July
15 July
20 July
21 July
22 July
25 July
27 July
28 July
OBS
BASE
BHNV
BHNJ
NIIR
EM97

Fig. 13

Fig. 13

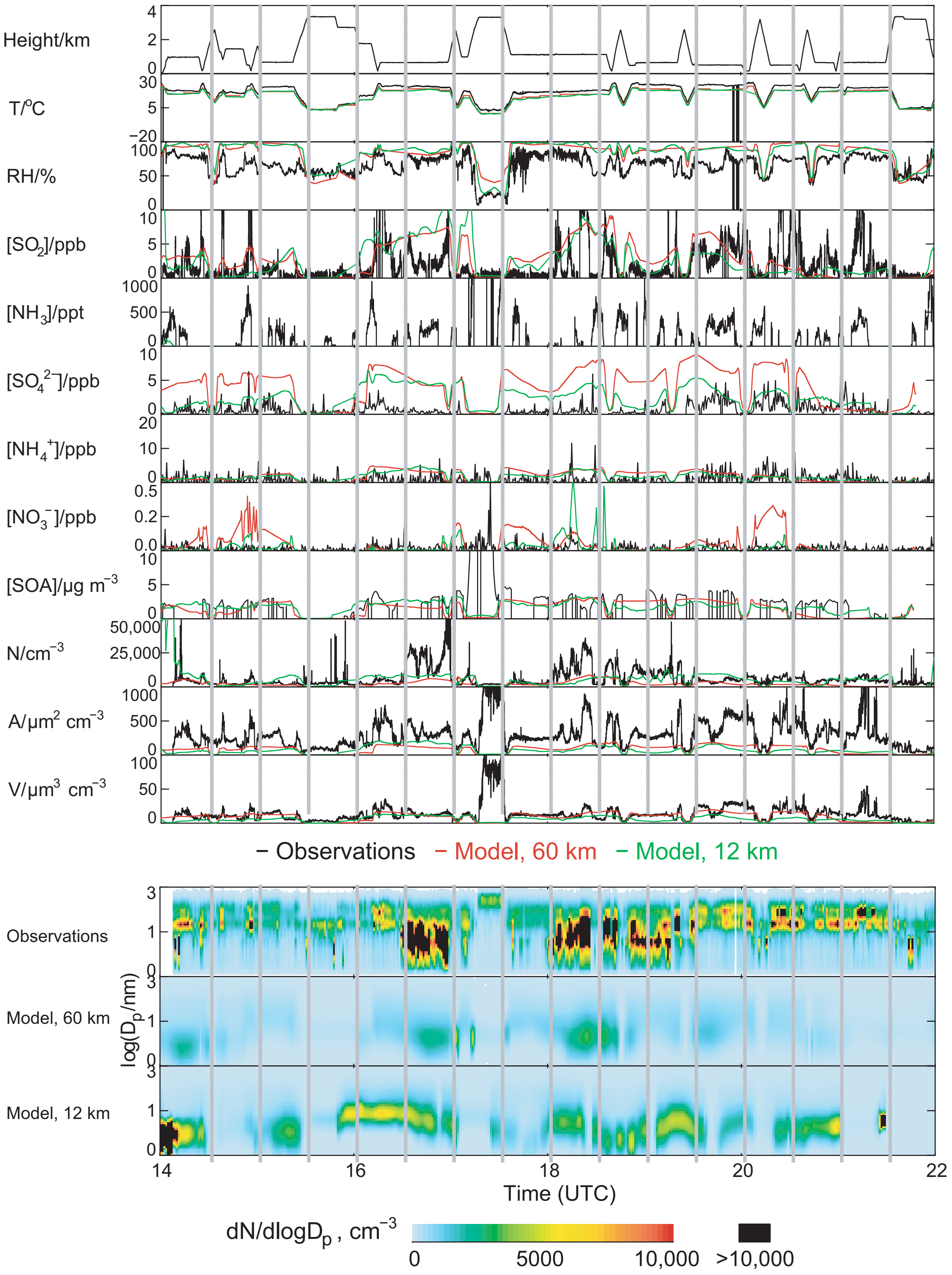

Height/km
0
2
4
T/°C
−20
5
30
RH/%
0
50
100
[SO$_2$]/ppb
0
5
10
[NH$_3$]/ppt
0
500
1000
[SO$_4^{2-}$]/ppb
0
5
10
[NH$_4^+$]/ppb
0
10
20
[NO$_3^-$]/ppb
0.0
0.2
0.5
[SOA]/μg m^{-3}
0
5
10
N/cm^{-3}
0
25,000
50,000
A/μm^2 cm^{-3}
0
500
1000
V/μm^3 cm^{-3}
0
50
100
− Observations
− Model, 60 km
− Model, 12 km
Observations
Model, 60 km
Model, 12 km
log(D$_p$/nm)
0
1
3
14
16
18
20
22
Time (UTC)
dN/dlogD$_p$, cm^{-3}
0
5000
10,000
>10,000